

Verification of Delft FLS

S.P.A. Duinmeijer



February 2002

TU Delft

Delft University of Technology



wl | delft hydraulics

Verification of Delft FLS

February 2002

Preface

The research described in this report was carried out as a graduation project to finish my studies in Civil Engineering at the Delft University of Technology in Delft, the Netherlands. The objective of this study was the verification of the computer model Delft FLS, which stands for Delft FLooding System. This model is developed at the WL | delft hydraulics and especially suited for the simulation of flooding.

I would like to thank the members of my graduation committee who gave me a lot of advice and useful comments, prof. dr. ir. G.S. Stelling, prof. dr. ir. J.A. Battjes, dr. ir. H.L. Fontijn and dr. ir. P.J. Visser. I also want to thank the members of the Fluid Mechanics Laboratory for realising my experimental set-up.

Finally, I would like to thank my family and friends for their support during this research.

Alex Duinmeijer

Delft, February 2002

Abstract

Nowadays flooding because of a dike breach can be simulated with high accuracy by use of computer models. *Delft FLS*, which stands for DELFT Flooding System, developed by WL | Delft Hydraulics, is such a model. The hydrodynamic processes occurring during a flooding are complex, for example moving hydraulic jumps and propagating bores. The implementation of the hydrodynamic laws in the computer model must be done correctly to be able to calculate these processes accurately.

To verify the accuracy of the model an experiment was developed and executed in which these hydrodynamic processes occurred. The experimental results were compared with the numerical results to allow statements about the accuracy of the model.

The experiment concerned the flooding of a basin of 8 m by 23 m. When a gate was lifted a reservoir emptied into the basin, which was thereby flooded. Three experiments were executed, two with different initial water layers in the basin and one with an initially dry basin.

A video camera above the basin recorded the development of the flooding in the horizontal plane. The water depths were registered with wave gauges.

The first numerical results seemed to agree reasonably well with the experimental data. However the calculated lateral flow velocity was too high. The dike-break is modelled in the computer program as a linear in time decreasing height of a dam. A numerical momentum conservative method is normally used in *Delft FLS* to calculate the flow through the breach. In the experiment a lifted gate represented the dike-break. The flow could not be calculated with the momentum conservative method because of a loss of momentum due to a force against the gate. An energy conservative numerical method is needed to calculate the flow. After applying the energy conservative numerical method the calculated results agreed very well with the experimental results.

Verification of the computer model *Delft FLS* showed that the numerical methods used in the computation core of the program are very suitable to calculate the complex hydrodynamic processes of flooding. The methods are mass, energy and momentum conservative, which results in very accurate computations of two-dimensional dynamic flow with discontinuities in it.

Samenvatting

Overstromingen ten gevolge van dijkdoorbraken kunnen tegenwoordig met behulp van computermodellen betrouwbaar gesimuleerd worden. *Delft FLS*, dat staat voor DELFT Flooding System, ontworpen door het WL | Delft Hydraulics, is een computermodel dat hiervoor speciaal ontwikkeld is. Bij een overstroming treden complexe hydrodynamische processen op, zoals bewegende watersprongen en voortplantende vloedgolven. Om deze processen nauwkeurig te kunnen berekenen is een juiste implementatie van de vloeistofmechanische wetten in het computermodel vereist.

Om de nauwkeurigheid van het model te controleren is een experiment ontworpen en uitgevoerd, waarbij deze hydrodynamische processen optraden. Om tot een uitspraak over de nauwkeurigheid van het model te kunnen komen werden de experimentele meetresultaten vergeleken met de numerieke resultaten.

Het experiment betrof een overstroming van een bassin van 8 meter breed en circa 23 meter lang. Door het heffen van een schuif stroomde water vanuit een reservoir het bassin in. Er zijn twee typen experimenten uitgevoerd. In het ene type experiment was het bassin aanvankelijk droog, in het andere type experiment was er een initiële waterlaag in het bassin.

Met behulp van een videocamera, gemonteerd boven het bassin, is de ontwikkeling van de overstroming in het horizontale vlak vastgelegd als functie van de tijd. Door middel van golfmeters zijn de waterstanden op verschillende locaties in het bassin en het reservoir geregistreerd.

De eerste numerieke resultaten van het model leken redelijk overeen te komen met de experimentele resultaten. Uit de berekeningen bleek echter dat de zijwaarts gerichte stroomsnelheid te hoog was. De dijkdoorbraak in het computermodel wordt gesimuleerd door middel van een afnemende hoogte van een dijk of dam. Voor het berekenen van de stroming door het ontstaande gat wordt normaal een numerieke impulsbehoudende methode in Delft FLS toegepast. In het experiment werd de doorbraak echter gesimuleerd door het een omhoog trekken van een schuif. De stroming kan in dit geval niet berekend worden met de impulsbehoudende methode, omdat er een verlies van (stromings-)impuls is als gevolg van een drukkracht op de schuif. Om de stroming in dit geval te berekenen is een energiebehoudende numerieke methode nodig. De berekende resultaten van de numerieke energiebehoudende methode kwamen nu zeer goed overeen met de experimentele resultaten.

Verificatie van het computermodel *Delft FLS* heeft aangetoond dat de gebruikte numerieke methoden in de rekenkern van het model zeer geschikt zijn voor het berekenen van de complexe dynamische processen die bij een overstroming optreden. De methoden zijn massa, energie en impulsbehoudend, wat resulteert in nauwkeurige berekeningen van twee-dimensionale dynamische stroming inclusief discontinuïteiten.

Contents

Preface	I
Abstract	II
Samenvatting	III
List of Figures	VI
List of Tables	VI
List of symbols	VI
1 Introduction	1
1.1 General	1
1.2 Problem description and research objective	2
1.3 Approach to problem	2
1.6 Overview of 2D dam and dike-break experiments in the literature	3
2 The physical experiment	7
2.1 Introduction	7
2.2 Set up of the experiment	7
2.2.1 Basic principle	7
2.2.2 Design parameters	8
2.3 Measuring techniques	11
2.3.1 Introduction	11
2.3.2 Wave gauges	11
2.3.3 Camera recording	13
2.4 Measuring program	13
2.5 Experimental results	14
2.5.1 Introduction	14
2.5.2 Measured water depths	15
2.5.3 Measured front bore positions	16
2.6 Duration of the experiments	16
2.7 Analysis of the results	17
2.7.1 Introduction	17
2.7.2 Wet bed experiment observations	17
2.7.3 Dry experiment observations	18
3 The Program Delft FLS	20
3.1 Introduction	20
3.2 The basic equations in the model Delft FLS	20
3.3 The numerical approximation of the shallow water equations in Delft FLS	21
3.1 Introduction	21
3.3.2 Conditions at discontinuities	22

3.3.3	Numerical approximation of the SWE in Delft FLS (Stelling, 1999).....	24
4	Verification of the numerical results.....	27
4.1	Introduction.....	27
4.2	Numerical results against experimental results for the wet-bed cases.....	27
4.2.1	Input parameters in Delft FLS	27
4.2.2	Numerical results for the 3 cm wet-bed case.....	28
4.2.3	Numerical results for the 5 cm wet-bed case.....	31
4.3	Numerical results against experimental data for the dry-bed case.....	33
4.3.1	Input parameters in Delft FLS	33
4.3.2	Numerical results for the dry-bed case.....	33
4.4	Conclusions drawn from the verification.....	36
5	Conclusions and recommendations	38
5.1	Conclusions.....	38
5.1.1	General.....	38
5.1.2	Practical.....	38
5.2	Recommendations.....	38
	References.....	40
	Appendices	41

List of Figures

Figure 1.1 Inundation of a village in Zeeland, 1953	1
Figure 1.2 Plan and side view of the CADAM test case. Dimensions in meters	4
Figure 1.3 Plan view of the experimental lay out (Fontijn and Kranenburg)	5
Figure 1.4 Water surface profiles (Fennema 1985)	6
Figure 2.1 Basic set-up of the experiment	7
Figure 2.2 Top view and side view of the experimental lay-out	9
Figure 2.3 Photo of the experimental set-up looking upstream	10
Figure 2.4 Experimental breach	11
Figure 2.5 Wave gauge	12
Figure 2.6 Camera image of the (dry) basin	14
Figure 2.7 Changing offset of a gauge	15
Figure 2.8 Average propagation speed of the wet-bed experiments	17
Figure 2.9 Average propagation speed of the dry-bed experiment.	18
Figure 2.10 Advancing wave front tip	18
Figure 2.11 Front bore positions on both halves of the basin	19
Figure 3.1 Discontinuity in a region of water	22
Figure 3.2 Staggered spatial grid	24
Figure 4.1 Calculated front bore positions and measured front bore positions, initial water depth 3 cm.	28
Figure 4.2 Calculated water depths and measured water depths, initial water depth 3 cm.	30
Figure 4.3 Calculated front bore positions and measured front bore positions, initial water depth 5 cm.	31
Figure 4.4 Calculated water depths and measured water depths, initial water depth 5 cm.	32
Figure 4.5 Calculated front bore positions and measured front bore positions, $n = 0.012 \text{ m}^{-1/3} \text{ s}$	33
Figure 4.6 Calculated front bore positions and measured front bore positions, $n = 0.010 \text{ m}^{-1/3} \text{ s}$	34
Figure 4.7 Calculated water depths and measured water depths (dry-bed case)	35

List of Tables

Table 2.1 Co-ordinates of the wave gauges	13
Table 2.2 Executed experiments	14

List of symbols

Roman symbols	Description	Unit
d	water depth below plane of reference	[m]
g	gravitational acceleration term	[m/s ²]
h	total water depth $h = d + \zeta$	[m]

h_b	water depth in the basin	[m]
h_r	water depth in the reservoir	[m]
r	radial coordinate	[m]
u	velocity in x-direction / radial flow velocity	[m/s]
v	velocity in y-direction	[m/s]
Q	volume flow	[m ³ /s]
q	volume flow per unity of width	[m ² /s]
t	time	[s]
n	Manning roughness coefficient	[m ^{-1/3} s]
k_s	Nikuradse roughness length	[m]

Greek symbols**Description****Unit**

ζ	water level above plane of reference	[m]
ξ	propagational speed of a bore	[m/s]
ρ	mass density	[kg/m ³]
ν	kinematics viscosity	[m ² /s]

I Introduction

I.1 General

The Netherlands are geographically situated in the delta of three rivers, the Rhine, the Meuse and the Schelde. These rivers have many distributaries through a great part of the country. Adjoining these rivers there are many villages and polders, used for living, working, recreation, agriculture and cattle breeding. These villages and polders are generally protected against flooding by dikes.

In the past many dike breaches occurred, resulting in the death of many people and animals, and significant economical losses. One of them is the 1953 flooding of the south-western part of the Netherlands, through more than two hundred dike breaches. This caused the death of 1835 people and a material damage of 1.5 billion Dutch guilders. Figure 1.1 gives an impression of the havoc and ravages committed.

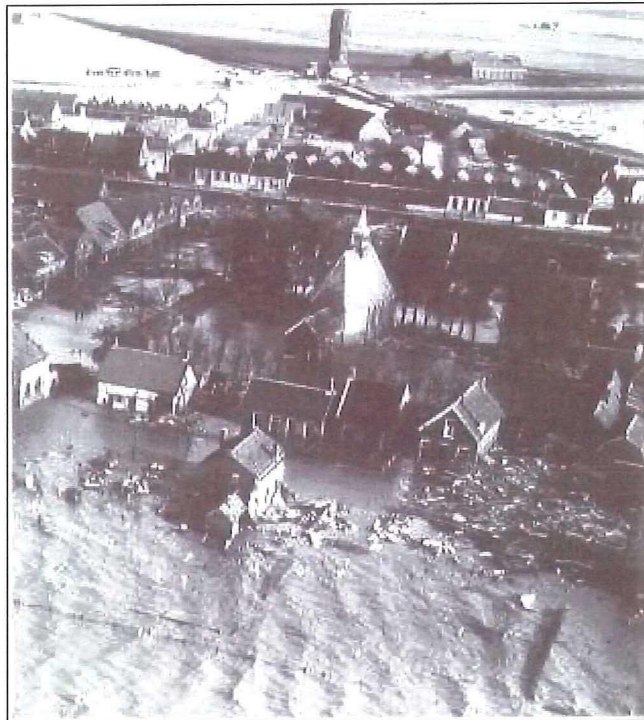


Figure 1.1 Inundation of a village in Zeeland, 1953

Recently in 1995, the water levels in the Rhine and the Meuse and its distributaries; the Waal, the Lek and the Boven Merwede rose to dangerous values, and by way of precaution about 250000 people were evacuated.

To prevent disasters like flooding, governments are extensively busy checking and heightening dikes. If a flooding would occur, the inundation generally causes great damage, and even loss of animal and human lives. If, against expectation, a flooding occurs, the development of the flooding is of interest for the authorities. Knowing the course, duration and expected depths of a flooding, calamity plans can be made to evacuate people and animals.

I.2 Problem description and research objective

The development of a flooding in a certain area can be calculated with numerical computer programs. Nowadays there are very powerful computers to run extensive models within an acceptable amount of time. Delft FLS, which stands for DELFT Flooding System, developed by WL | DELFT Hydraulics, is such a computer program to simulate flooding, for instance after a dike or dam-break.

To simulate a flooding event accurately, many aspects are to be taken into account like the size and growth of the breach, the effects of small canals and ditches, the presence of urban areas with streets and buildings and the effects of small dams and elevations in the field e.g. railroads. For accurate results each aspect needs separate verification and validation. Some of these aspects are related mainly to process formulation, for example the flow over cropland or through bushes and trees. The flow can be considered here as a diffusive wave that is friction dominated. The accuracy is mainly determined by the friction formulation and depends on the input data.

Other very important aspects are related to the numerical approximation methods of the conservation laws in the program. The accuracy of the calculated flow is highly dependent on this approximation. A severe test for the accuracy of the numerical approximation in the program is the calculation of dynamic flow with discontinuities in it, like hydraulic jumps and moving bores.

To determine the accuracy of the numerical approximation, the numerical results of the computer program must be verified. This can be done by comparing data obtained from physical experiments with the numerical results. De Vries (1999) verified the computational core of the program Delft FLS successfully by applying different analytical solutions of one-dimensional dam-break problems with shocks in the flow and data obtained by semi two-dimensional¹ experiments, representing dam-breaks with discontinuities in the flow. The results of this verification were satisfying. The experiments were however semi two-dimensional: they represented the flow after a hydro dam-break in a narrow valley (see also section 1.4). After a dike-break, however, the downstream flow is usually into a wide flat polder, as supposed to a dam-break flow into a channeled valley. The dike-break flow is thus much more two-dimensional. The computational core of the program needs verification also for this dynamic phase of a flooding.

So, the problem is that the accuracy of the numerical approximation of the SWE² in Delft FLS in case of calculating two-dimensional dynamic flow including discontinuities has never been determined.

The objective of this research is thus the verification of the numerical approximation of the SWE in case of unrestricted two-dimensional dynamic flow including discontinuities.

I.3 Approach to problem

To verify the computational core of the program in case of two-dimensional dynamic flow, experimental data is needed. This data is obtained by the experiments described in this report. The experimental set-up has to provide discontinuities in a two-dimensional flow. These discontinuities could occur by a flooding over initial dry land as well as land covered with an initial water layer. At the first event the transition of dry to wet at the front of the wave can be seen as a discontinuity. At the latter event, hydraulic jumps and bores are considered as discontinuities in the flow. The experiment has been

¹ two-dimensional in the horizontal plane

² Shallow Water Equations

designed such that both events could be executed. The measurement data, obtained through the experiments, must provide information concerning the characteristic properties of the events, like;

- The form of the front bore in the horizontal plane;
- the height and location of the hydraulic jump;
- the development of the bore propagation speed;
- the development of the water depths at different positions behind the dike;
- the volume flow through the breach.

The calculated results will be compared with the experimental results. This verification gives information concerning the accuracy of the numerical approximated SWE in the computational core of Delft FLS for the dynamic phase of a flooding.

1.6 Overview of 2D dam and dike-break experiments in the literature

A literature search concerning dam- and dike-break flows yielded many studies and experiments about one-dimensional flows, such as flow into a channelled valley downstream of a (hydro-) dam. There are hardly any data available concerning two-dimensional flow (2Dh) into, for example, a polder after a dike-break.

The studies mostly concern flow simulating with numerical (computer) models. The following overview shows the most relevant experiments, and they will be discussed briefly.

Overview experiments

Experiment / study	Description
De Vries (1999)	Flooding, Classification and simulation
CADAM cases (1998)	Experimental dam-break flow into a channel with a 45° bend
Fontijn and Kranenburg (1985)	Experimental (axial symmetric) flood wave propagation after a dike-break
R.F. Fennema (1985)	Two-dimensional (2Dh) dam-break flow experiments and comparison with a numerical model
Dressler (1975)	One-dimensional dam-break flow experiments to determine the acceptability of the Chezy resistance function

CADAM test cases / de Vries

In february 1998 CADAM - the European Concerted Action of Dam-break Modeling - was started. It was intended to exchange information on dam-break modeling between Universities, Research Organizations and Industry. One of the specific objectives is the creation of a database of test cases (analytical, experimental and real life) available for reference. Difference approaches to the numerical simulation of flow after a dam failure have been compared to the experimental data in the database. The experiments combine different properties of dam-break flow that have proven difficult to simulate accurately.

One of the test cases was a dam-break flow into a channel with a 45° bend, see Figure 1.2. The model combines a square shaped reservoir upstream and a prismatic channel. The flow will be essentially 2D in

the bend region between the two reaches of the channel. This test case has some interesting properties of the dam-break flow. One of them is the upstream moving hydraulic jump, which forms at the bend. For the exact set-up of the experiment and the data of the measurements, see Soares (1998). De Vries (1999) compared the measurement data with the calculated data for verification of the program Delft FLS. He did this for initially dry and wet bed cases. He concluded that the computation core in the program gives qualitatively good overall results when simulating flow over initially dry and wet bed of the CADAM test case.

De Vries also compared the results of an analytical exact solution of a 1Dh dam-break flow with the simulation results for both the dry and the wet bed case. The analytical solution is based on Stoker (1957). Both the test cases were calculated correctly by Delft FLS.

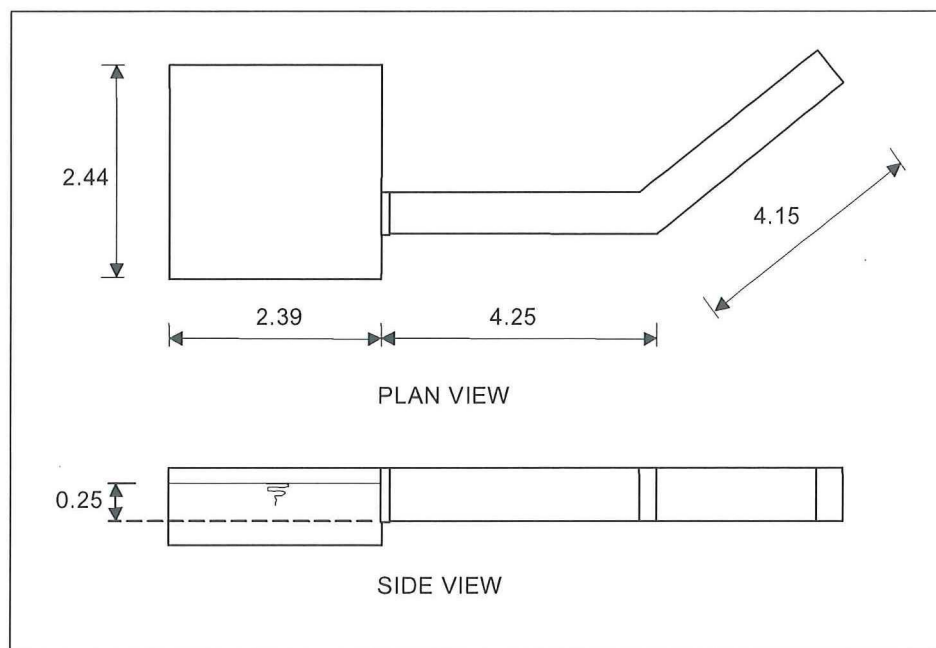


Figure 1.2 Plan and side view of the CADAM test case. Dimensions in meters

Fontijn and Kranenburg

Fontijn and Kranenburg (1985) did some dike-break experiments at the Fluid Mechanics Laboratory, Delft University of Technology, the Netherlands. The motivation for the experiments was to obtain insight in the radial symmetric flow and wave propagation into a lake after a dike-break. Because of the symmetry of the radial flow after a dike-break with respect to a vertical plane, the physical model represented only one half of the dike-break, see Figure 1.3. A lifted vertical gate simulated the break. The gate could be lifted with two different speeds. Two physical models were used, one model to obtain insight in the wave propagation near the dike-break and a circle-sector model to simulate the axial-symmetric wave propagation into the far field. The last model used a vertical wall such that the 'flooded' basin had the shape of a circle-sector. A dotted line in Figure 1.3 represents this wall. The basin represented the lake and the reservoir a storage basin. The water depth reservoir remained constant. The following parameters were varied: the water depth in the basin, the water depth in the reservoir, the mass-flow through the orifice and the lift-speed of the gate.

Fontijn and Kranenburg concluded that the first physical model showed a distinct moving hydraulic jump (bore), while the circle-sector model showed it much less. The first model also established a 90 degrees

angle of the moving hydraulic jump with the symmetric axis. The height of the hydraulic jump is dependent weakly of the water depth in the reservoir, but is depended strongly on the mass-flow through the orifice. A higher lift-speed gives also a higher hydraulic jump. The assumption that the flow is axial-symmetric was fully legitimate. Both physical models displayed this.

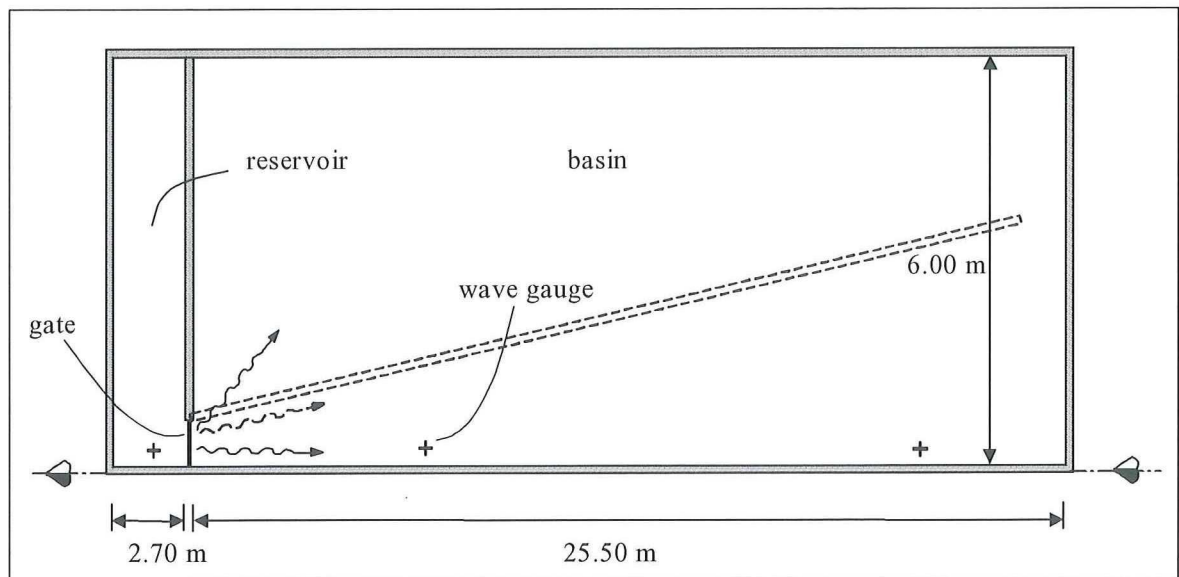


Figure 1.3 Plan view of the experimental lay out (Fontijn and Kranenburg)

Fennema

Fennema (1985) numerically analysed transient free-surface flows from the breaking of a dam. The numerical solutions were compared qualitatively with experimental results, performed in a laboratory flume at the Albrook Hydraulics Laboratory, Washington State University.

The data obtained in these experiments were used for *visual* comparison with a numerical model. The basic dimensions of the flume were a length of 8.06 m and a width of 1.22 m. A wood structure sandwiched between a plywood exterior served as the model of a dam with its centre located 2.61 m from the upstream end. A sheet of plexiglas served as a gate and was made to slide in Plexiglas grooves installed in the centre of the dam. The gate had a width of 0.28 m. The experimental procedure was as follows: the flume was filled with water until the desired tailwater level was reached, the gate was inserted and the upstream portion was filled until the desired reservoir level was reached. The flume was filled to a water level of 0.1 m. The reservoir was filled to a water depth of 0.7 m. The water surface profiles, following the simulated dam-break, were documented by a 35 mm camera that had the capacity to automatically record four frames per second. No precise timing mechanism was available at the time of these experiments. The photographs were made with a tolerance of ± 0.2 s of their time sequence. The variation in time of each photographic sequence made that a quantitative comparison of wave front location between physical and computational runs cannot produce useful results. Only qualitative comparisons of wave height and waveform could be made. Fennema assumed that the Manning roughness value for the physical model is $n = 0.014 \text{ m}^{-1/3}\text{s}$, representative of a bottom of smooth concrete.

As stated above, only visual comparison could be made between the results of computational runs and the physical results. Figure 1.4 shows the computational results of the water surface profiles at 0.25 s, 0.5 s and 0.75 s, after the start of lifting the gate.

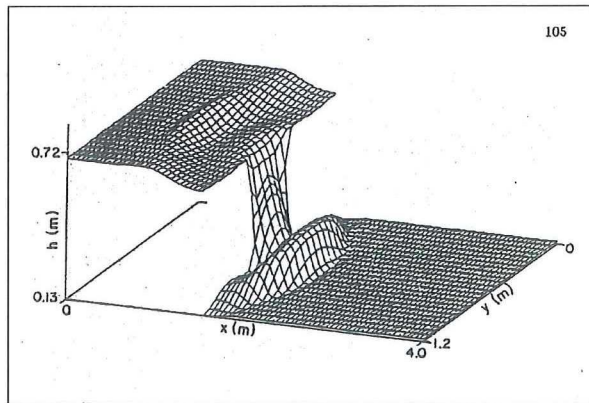
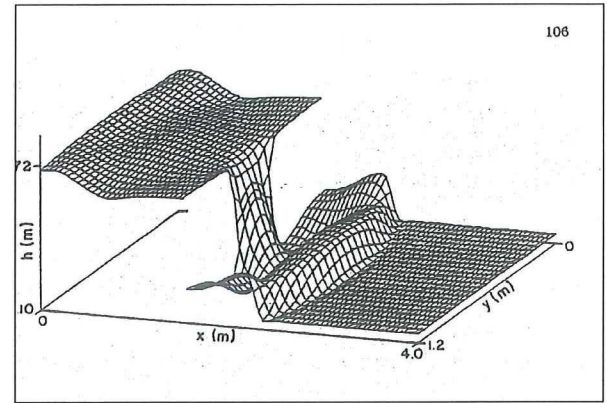
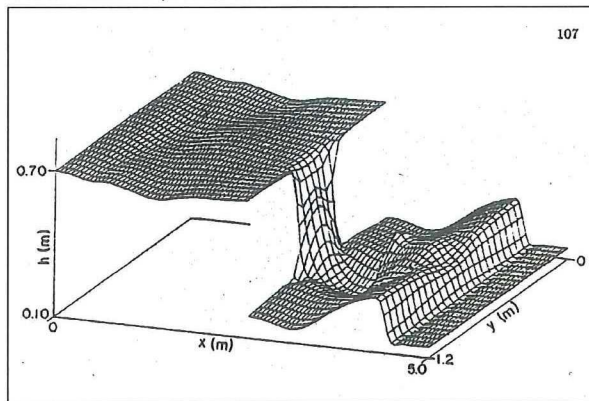
Water-surface profile at $t = 0.25$ sWater-surface profile at $t = 0.50$ sWater-surface profile at $t = 0.75$ s

Figure 1.4 Water surface profiles (Fennema 1985)

The computational results of water surface profiles compared visually well with the water surface profiles of the physical experiments. However, this experiment provides no exact measured information about the propagation speed of the wave front and the position of the wave front in the horizontal plane as function of time. The width of the flume was, compared to the width of the gate, too small to determine the development of the lateral flow.

Dressler

Dressler (1975) compared theories and experiments for the hydraulic dam-break wave. The experiments were one-dimensional in the horizontal plane. The one-dimensional character of the flow is not of interest in the frame of this study. The main object of the Dressler experiments was to determine the validity of several resistance formulations in the SWE in case of a dam-break flow or any other highly unsteady flow. The results of this study could be of importance in the verification of the computer program Delft FLS. The results of this study will be discussed in chapter 4.

2 The physical experiment

2.1 Introduction

The physical experiment represents a flooding of a flat, horizontal area after a dike-break. It was performed in January and February 2001, at the Fluid Mechanics Laboratory, Faculty of Civil Engineering and Geosciences, Delft University of Technology, The Netherlands.

Section 2.2 describes the set-up of the experiment. It describes and explains the choices made in designing and setting up the experiment. Section 2.3 describes the set-up of the experiment. Section 2.4 presents the measuring program.

2.2 Set up of the experiment

2.2.1 Basic principle

The experimental set-up consisted of two reservoirs, side by side with different water levels, separated by a wall. In the middle of the wall is a gate, which can be lifted in vertical direction. A rectangular aperture is generated in the wall when lifting the gate. The procedure of lifting the gate is meant to represent a dike-break. The typical mechanisms of dike-break and breach growth were not taken into account. The breach had a constant width.

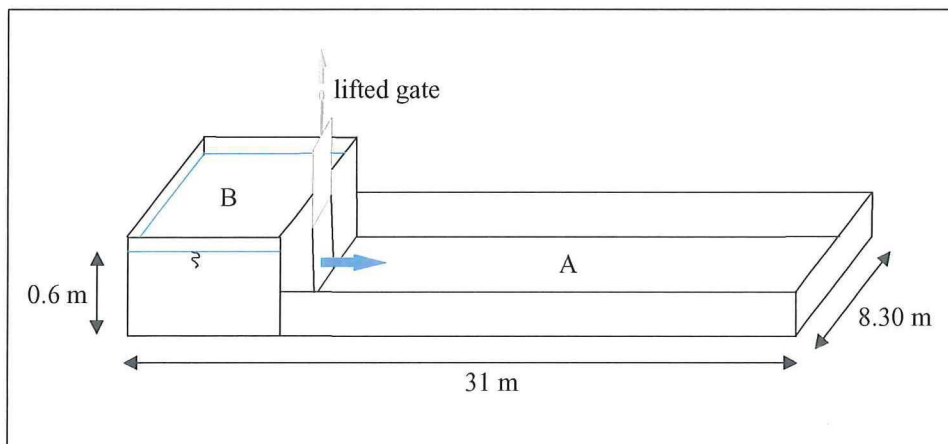


Figure 2.1 Basic set-up of the experiment

When lifting the gate, one of the reservoirs flooded (A), while the other (B) emptied itself, see Figure 2.1. The first question was whether a constant water level in the filled reservoir (B) should be maintained or not. In case of a real dike-break, the water level of a river, for example, does not fall when losing water through a breach into a near polder. Nevertheless, in case of this experiment a choice was made for an emptying reservoir. By measuring the water-level decrease in the reservoir in time, one can determine the mass flux through the aperture. Measuring the mass flux through the aperture with instruments would be difficult and inaccurate.

2.2.2 Design parameters

The experiment was designed to produce dynamic two-dimensional flow events, in our case flooding of a flat horizontal area after a dike-break. The space available for the experiment was a rectangular basin, 31 m long and 8.30 m wide. This basin had a smooth surface of concrete reinforced with synthetic fibre. The long side of the basin was chosen in the main direction of the propagating wave front. The reason for this choice was that the wave front could propagate undisturbedly along the centreline of the basin over about 29 m. The other choice would yield a propagation distance of about 8 m. This was too short to gather useful information, for example, on the influences of bottom friction on the propagation speed of the wave front.

The choice of the length of the reservoir (B) had a restriction. The volume of water in the reservoir must be large enough to give a dynamic overland flow at the initial stage of the experiment. If the water volume in the reservoir was too small, the pressure gradient in the aperture should decrease too fast at the specific time scale of the experiment. If this should happen, one could not speak of dynamic flow. With the program Delft FLS some simulations were made to determine the influence of the reservoir size. The results from the simulations with a reservoir length of 0.5 m and a reservoir length of 2 m showed a significant difference in the dynamic time scale. This resulted in a reservoir width of minimal 2 m.

The width of the gate was set at 0.40 m. A large width would reduce the available space to flow sideways. The water level in the reservoir was set at 0.6 m.

The type of experiments with an initial water depth in the basin was divided into two parts. One experiment had a water depth of 3 cm in the basin and the other experiment had 5 cm initial water depth in the basin.

The choice of the initial water depth in the basin was rather restricted. If the initial water depth in the basin is too large, for instance if the ratio h_b/h_r between the basin water depth h_b and the reservoir water depth h_r is about 0.5, the flow is subcritical everywhere (Fennema, 1985).

Zoppou et al. (1998) suggested that much smaller ratios give supercritical flow, which is a much more severe test for numerical schemes. The wet-bed experiment is executed with the small ratios of 0.083 and 0.05. The reason of the bipartition in the ratios was to determine the influence of this on the results of the numerical model.

Figures 2.2 and 2.3 show the design of the lay-out of the experiment and its practical execution, respectively.

The gate was lifted by using a crane with a constant lifting speed of about 16 centimetres per second. This was the maximal lift speed of the crane. Lifting the gate by use of a crane was carried out successfully before by Fontijn and Kranenburg (1985) in their physical experiments. Using the crane was very practical because no complicated lift construction with heavy fall-weights was necessary.

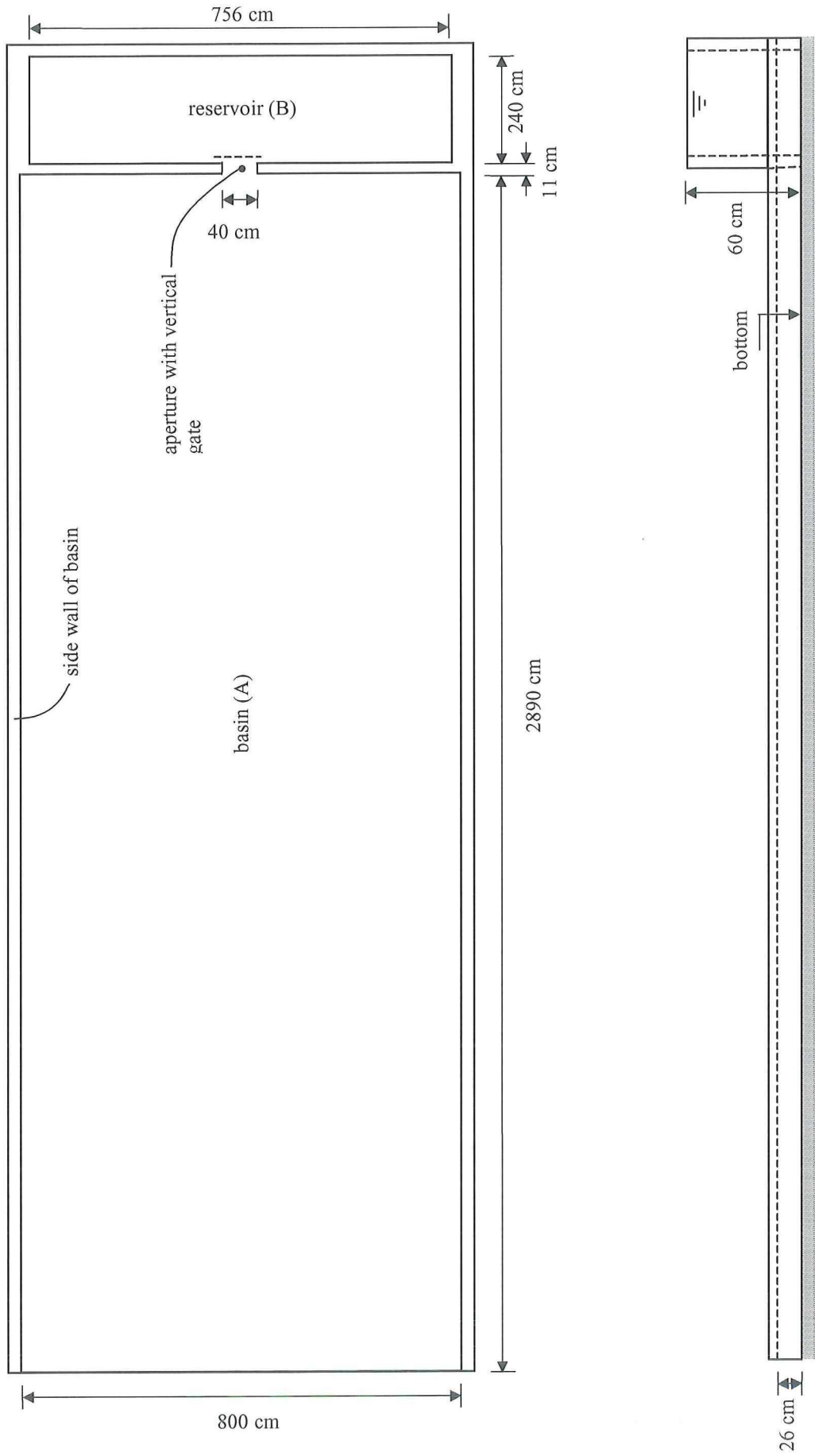


Figure 2.2 Top view and side view of the experimental lay-out



Figure 2.3 Photo of the experimental set-up looking upstream



Figure 2.4 Experimental breach

2.3 Measuring techniques

2.3.1 Introduction

Section 1.3, chapter 1 describes what data was measured from the physical experiments. This concerns:

- The development of the water depths at different positions behind the dike;
- the development of the water depth in the reservoir;
- the development of the wave propagation speed;
- the form of the front bore in the horizontal plane.

The development of the water depth at different positions in the basin and reservoir can be measured with so called “*wave gauges*”. These register a change in water depth as function of time. They also measure the moment that a propagating wave passes the location of the gauge.

The form of the front bore in the horizontal plane can be measured with a video-camera. This video-camera records the development of this front bore as a function of the time.

2.3.2 Wave gauges

Water level measurements were done with resistance wave gauges, see Figure 2.5. The principle of these gauges is based on the conductivity of water: a water level change is equivalent to a different resistance.

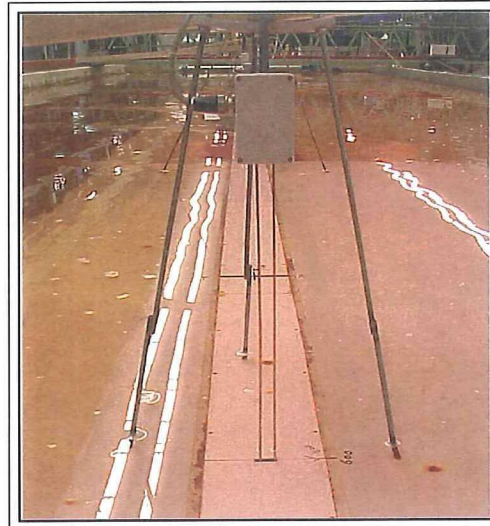


Figure 2.5 Wave gauge

The output signal of the gauge is a voltage. A data-acquisition system with an ADC (analogue-digital converter) samples the signals of the respective gauges synchronically with a frequency of 500 Hz and stores it. In other words: every 0.002 second the signals of the gauges are stored. The of the system is adjustable. A sample rate of 500 Hz was chosen for the experiment, which was high enough to resolve the shape of the wave.

The measured electric potential of a gauge is representative for a water level. This output signal had to be converted to a water level. The signals therefore were multiplied with a calibration-value. Each gauge has a calibration value of its own. The calibration values of the wave gauges were determined for each experiment as a relation between a static water level difference and a difference in signal. The lower parts of the wave gauges were placed in a trench in the bottom of the basin because the wave gauges had to maintain contact with water over a minimum length for a correct working. The trench was filled with water up to the level of the bottom of the basin.

Positions of the wave gauges

The wave gauges were not suitable to measure the form of the front bore in the horizontal plane as a function of time, which was one of the unknowns in the experiment. So, the wave gauges were only used for measuring the propagation speed and the height of the wave front. Seven gauges were placed in the basin (A), and one wave gauge was placed in the reservoir. The gauges had the following horizontal co-ordinates, with the origin of the co-ordinates at the centreline of the gate, The positive x-direction is downstream. The y-co-ordinates of the gauges are zero because they are placed along the centreline of the basin and reservoir.

gauge number	x-co-ordinate	position
00	-1	reservoir B
01	1	basin A
02	6	"
03	9	"
04	13	"
05	17	"
06	21	"
07	23	"

Table 2.1 Co-ordinates of the wave gauges

2.3.3 Camera recording

A Kodak digital video-camera was applied to record the spatial flow profile in the horizontal plane. This video-camera recorded at a frequency of 30 Hz. Each image was saved each on the hard disk of a personal computer. The video-camera recorded only a part of one half of the basin. This was justifiable because the flow was observed to be symmetrical with respect to a vertical plane through the lengthwise axis of symmetry of reservoir A. The video-camera was placed a few meters above the experimental basin. The recorded area was large enough to see the sideways propagation of the front until it reflected against the basin wall. A part of one half of the basin floor was painted white to get a better contrast between the wave and the floor, and the water was coloured red to enlarge this contrast. See also Figure 2.3.

A black cross with known co-ordinates was marked on the floor of the recorded area. This was done to determine the position of the recorded wave front in the basin at every moment. A digital stopwatch is placed in front of the camera to register the time corresponding to the recorded images.

Figure 2.6 shows the recorded image of the part of one half of the basin. Point (a) inside the Figure shows the black cross and point (b) shows the stopwatch. The circumscribed part at point (b) inside the Figure is enlarged and placed in the right corner of the Figure.

2.4 Measuring program

Two types of experiments were performed. In one type of experiment the basin was initially dry; the other type comprised the experiments with an initial water depth in the basin.

The first three experiments with zero initial water depth were used to investigate the reproducibility of the experiments. The three experiments were compared to each other and this resulted in three identical forms of the front bore. The decision was made to execute each type of experiment only twice, just to notice some possible unexpected measuring results.

The type of experiments with an initial water depth in the basin was divided into two parts. One experiment had a water depth of 3 cm in the basin and the other experiment had 5 cm initial water depth in the basin. Table 2.2 shows the labels of the executed experiments.

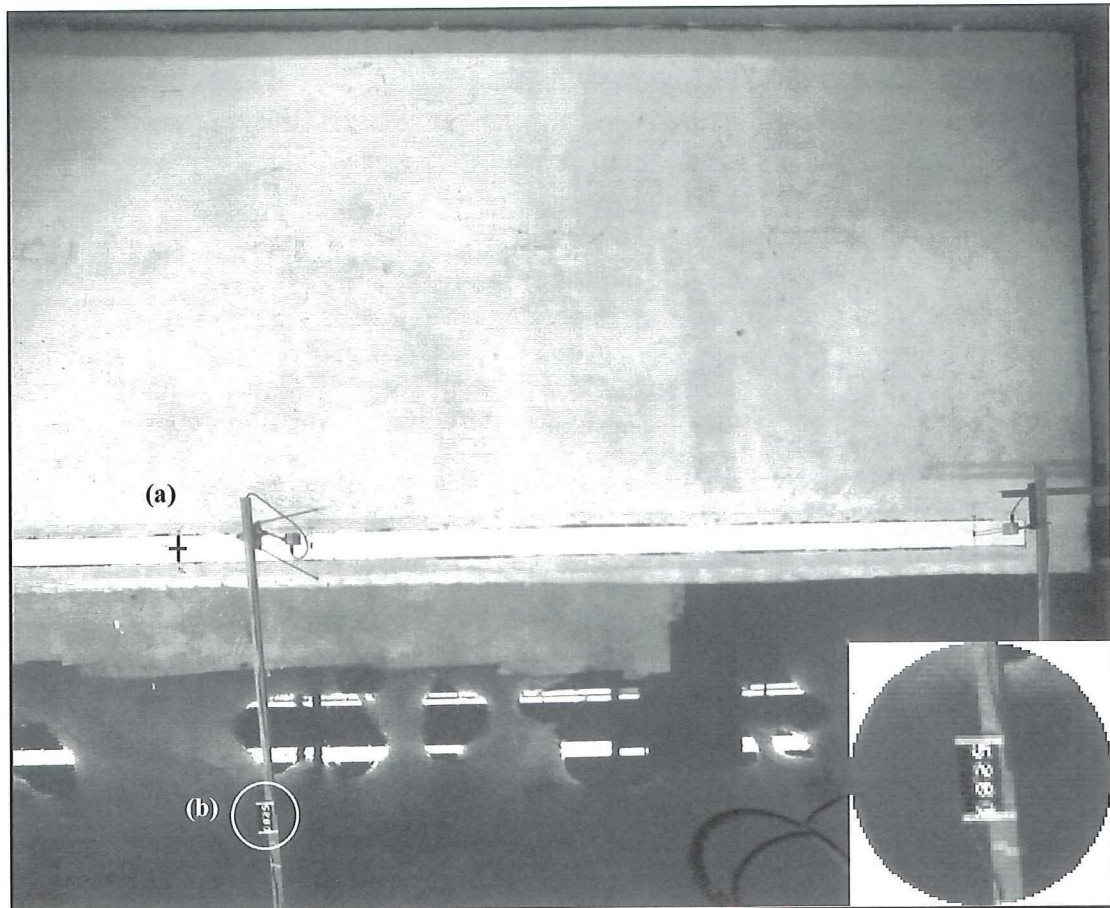


Figure 2.6 Camera image of the (dry) basin

Experiment name	Initial water depth
Exp06	0 cm (dry bed)
Exp07	0 cm (dry bed)
Exp08	3 cm
Exp09	3 cm
Exp12	5 cm
Exp15	5 cm

Table 2.2 Executed experiments

2.5 Experimental results

2.5.1 Introduction

Through analysis and discussion of the results, one can determine which experimental data were useful to verify the numerical model.

Section 2.5.2 describes the results of the wave gauges. Section 2.5.3 describes the location of the front bore in the horizontal plane measured by camera. Section 2.5.4 contains the duration of the experiments.

2.5.2 Measured water depths

Appendix A shows the measured water depths for both the dry- and wet-bed experiments.

The vertical arrows in the graph, with wave gauge number, indicate the moment the wave front reached the wave gauge concerned. An almost vertical line in the development of a water depth signifies this.

During the dry bed experiment the recordings of wave gauges 03 and 04 did not allow to measure the complete height of the wave (see the horizontal lines in appendix A). This was caused by a combination of offset and installed measuring range of the gauges. The initial start settings of the gauges were meant to measure the highest water level occurring. But, before the first wave front had reached the gauge considered, its offset value increased and with this the measuring range decreased. How this could happen, can be explained as follows. The lower parts of the gauges were placed in a trench in the bottom of the basin, see Figure 2.7.

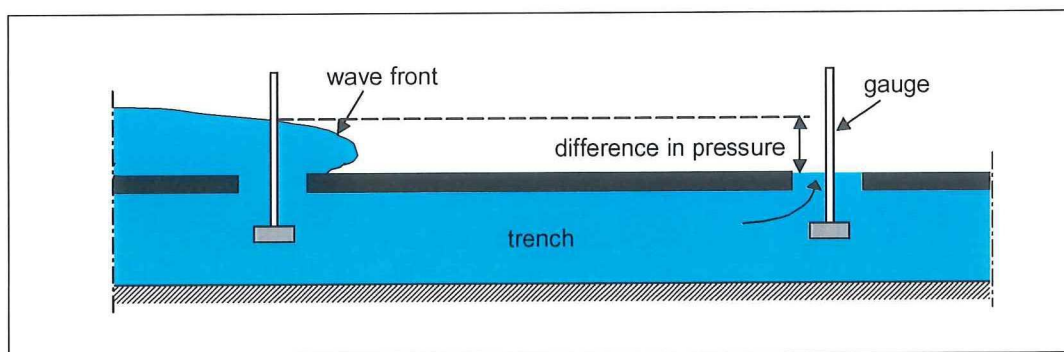


Figure 2.7 Changing offset of a gauge

The trench was filled with water up to the level of the bottom of the basin, as the gauges at their lower parts had to maintain contact with water over a minimum length. When the wave front reached the first gauge in the basin, the pressure in the trench increased. This caused a pressure wave propagating in the trench. The wave pushed the water up through the gap around the next gauge bars. Because of this phenomenon the measuring range of the wave gauges is reduced. This phenomenon is observed at a video film where one could observe that water was pushed out of the gaps before the wave front had reached this wave gauge. Closing up the trench between the gauges could solve this problem. But the physical experiment was already pulled down when the problem was discovered.

The measured data of the gauges 03 and 04 could only be used for information about the propagation speed of the wave front and the reflected wave.

Before the start of the wet bed experiments several gauges showed oscillating offset values. These values must be constant before starting the measurements. If an offset value is not constant, inaccuracy of the measured values occurs. A possible reason could be fluctuation of the water surface in the (filled) basin. The wave gauges did not oscillate at the dry-bed experiments, which suggests again the possibility of a fluctuation of the water surface, although this is not observed visually.

Some offset values were oscillating with amplitudes of 2.5 V. Such an electric potential difference corresponds to a water level elevation of 1.25 cm. This can lead to large measuring errors. For instance, if one expects a bore of 5 cm height, the measurement error can be 25 percent. To avoid this, the following solution is applied to the oscillating offset values. The average value was calculated for each gauge before the start of the experiment:

$$\bar{x} = \frac{1}{n} \sum_{i=1}^n x_i \quad (2.2)$$

where n is the number of measurements, 24501, before the experiments started and x is the measurement value. By calculating the standard deviation of the same data set, one can determine the variability of this set:

$$\sigma = \sqrt{\frac{1}{n} \sum_{i=1}^n (\bar{x} - x_i)^2} \quad (2.3)$$

The highest standard deviation was 0.41 V. One could make an indication of the measured relative error: 0.41 V corresponds to an elevation of $0.41 \text{ V} * 0.5 \text{ cm/V} = 0.2 \text{ cm}$. The average elevation of gauge 02 at the experiment was about 3 cm. Thus, an indication of the maximal relative standard error in the measurements due to errors in the offset was about 6.7 percent.

2.5.3 Measured front bore positions

Appendix B shows the location of the front bore in the horizontal plane measured with the video-camera at times $t = 1 \text{ s}$, $t = 2 \text{ s}$, $t = 3 \text{ s}$ and $t = 4 \text{ s}$ after the start of lifting the gate. The front bore positions of the dry bed experiment are contoured with a grey line for a distinct difference between dry and wet surface.

The program L&C Arith, developed at the Fluid Mechanics Laboratory, Faculty of Civil Engineering and Geosciences, Delft University of Technology, can convert camera images into Cartesian co-ordinates. These co-ordinates can be used in programs that can make graphs, like Excel. Two points at a camera image need to be known in co-ordinates of an orthogonal co-ordinate system, see section 2.3.3.

Appendix C shows the resulting location of the front bore at times moments $t = 0.5 \text{ s}$ through $t = 4.5 \text{ s}$ after lifting the gate with steps $\Delta t = 0.5 \text{ s}$.

2.6 Duration of the experiments

The duration of an experiment was equal to the time between the start of lifting the gate ($t = 0 \text{ s}$) and the moment the wave front reached gauge number 07. This gauge was located at a distance of 23 meter from the aperture. Behind this gauge, the water flowed away into a storage tank. By analysing the measurements, one can determine the moment the wave reached this gauge.

The duration of the initial dry experiment was about 26 seconds. The experiment with an initial water depth of 3 cm had a duration of 19 seconds, whereas the experiment with a depth of 5 cm took 18 seconds.

2.7 Analysis of the results

2.7.1 Introduction

By analysing the results of the wave gauges and the video-camera, one could see distinct differences between the two types of experiments.

Section 2.7.2 discusses the observations made with the video-camera in the experiments with initial water depths of 3 cm and 5 cm. Section 2.7.3 treats the observations made in the dry-bed experiment.

2.7.2 Wet bed experiment observations

The propagation speed of the wave front is calculated using the front bore positions from Appendix C. The speed of propagation is calculated by dividing the distance travelled by the wave front (in longitudinal direction) with the duration of it:

$$\bar{\xi}(t) = \frac{x(t)}{t} \quad (2.4)$$

with $x(t)$ the location of the wave front at time t ($t = 0$ s at the start of lifting the gate). Figure 2.8 shows the average speed of propagation of the wave front:

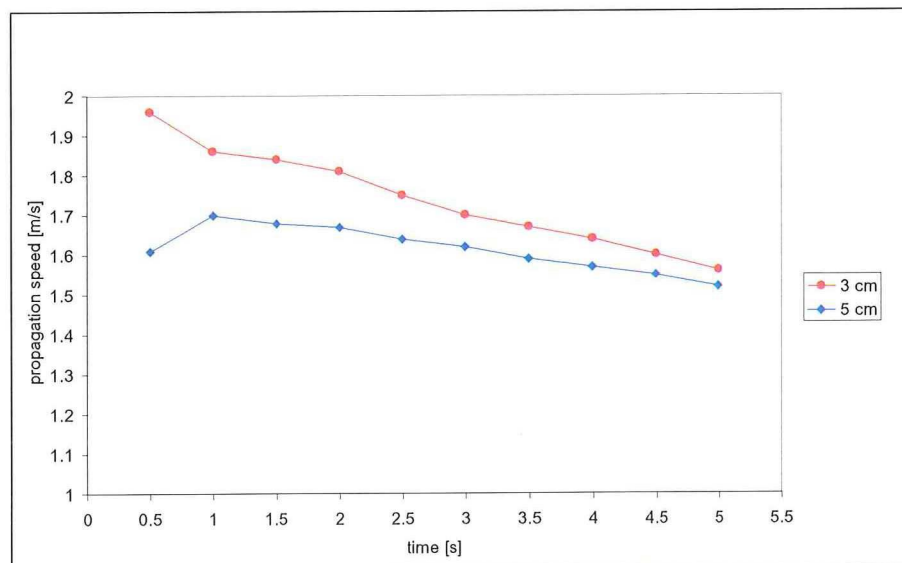


Figure 2.8 Average propagation speed of the wet-bed experiments

It can be seen in the Figure that the propagation speed in the initial 5 cm wet-bed experiment is lower than the propagation speed in the 3 cm initial wet-bed experiment. The main reason for this difference is that the wet-bed experiment, with a greater initial water depth downstream, transfers more momentum to the downstream water layer than to a shallower water layer downstream. This transfer of momentum is needed to actuate the still water downstream of the aperture.

2.7.3 Dry experiment observations

The propagational speed of the wave front is calculated in the same way as was done in section 2.7.2, by using the front bore positions presented in Appendix C. Figure 2.9 shows that the average speed of the wave front is decreasing with increasing time. The influence of the bottom friction, which in case of the wet-bed experiments was not of great importance compared to the transfer of momentum to the downstream water layer.

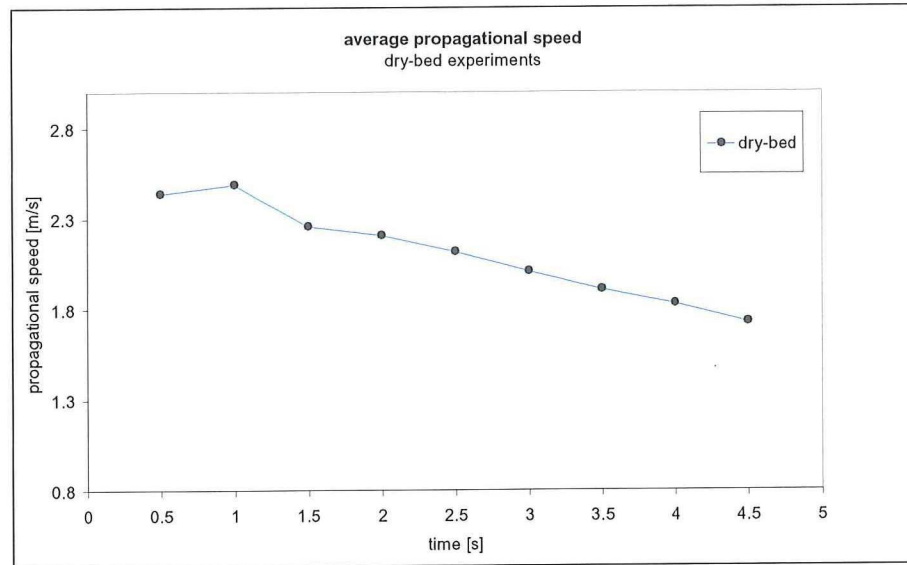


Figure 2.9 Average propagation speed of the dry-bed experiment.

The influence of the bottom friction can be visually demonstrated by recorded images of the front bore positions from Appendix B. If one takes a closer look at the propagating wave front on the cover of the trench in the basin, it can be observed that here the wave front advances faster, see Figure 2.10.

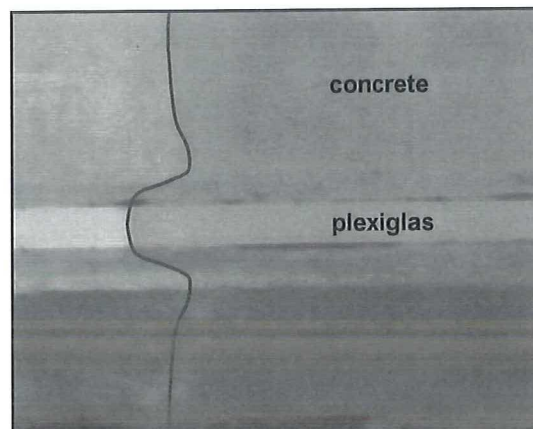


Figure 2.10 Advancing wave front tip

The cover of the trench is made of plexiglas, which is a smooth material. The floor of the basin is made of concrete, which is much rougher. This implies that the bottom roughness, hence the bottom shear stress, plays a part in the propagation speed of the wave front.

That this consideration is correct can be proved by the difference in front bore positions on both halves of the basin. The surface of one half of the basin is painted white (see also Figure 2.6). Figure 2.11 shows the front bore positions on both halves of the basin.

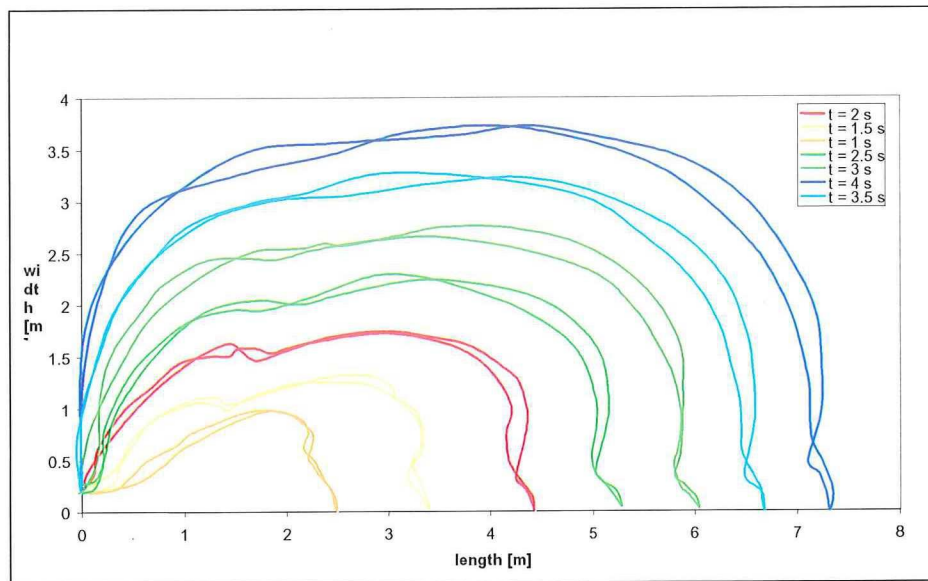


Figure 2.11 Front bore positions on both halves of the basin

The outermost lines represent the front bore positions on the white painted floor and the inner lines represent the front bore positions on the unpainted opposite surface. Thus, the propagation speed of the front on the white painted surface is higher than on the unpainted surface! Apparently, the white painted surface is less rough than the unpainted surface. This again indicates the influence of the bottom friction on the wave profile.

Additionally, this also implies that the concrete of the basin is relatively smooth. This because of that the unevenness of the concrete can be flattened out by a thin layer of paint.

In conclusion, one has to take good notice of the importance of the bottom friction even in a highly dynamic flow that following a dike-break.

3 The Program Delft FLS

3.1 Introduction

High population and economic activities near rivers have increased the need for reliable flooding prediction, flood calamity plans and flooding damage assessment. A reliable prediction of the hydrodynamics of the flooding is obviously needed to fulfill these assignments.

Delft FLS is a hydrodynamic prediction program developed by the WL | Delft Hydraulics, Delft, The Netherlands. The program is suited to import GIS data (Geographical Information Systems) into the model and to export computational results to GIS systems for professional presentations and evaluation. This makes the program a very useful and easy simulation tool. The program is especially suited to simulate the dynamic behaviour of overland flow over initially dry land, as well as flooding and drying processes on every kind of geometry, including lowlands or mountain areas. It simulates the influence of the existing / planned infrastructure on flooding processes. Land use, vegetation characteristics and urban areas are also included. Internal boundary conditions are included to simulate dam-break / dike-break events.

This chapter describes the equations used in Delft FLS. Section 3.2 describes the basic equations in the model. The subsequent section describes the numerical discretization of the equations.

3.2 The basic equations in the model Delft FLS

Delft FLS simulates unsteady hydrodynamic flow in two dimensions. It computes flow using the two-dimensional shallow water equations on a rectilinear grid, based on a robust finite difference scheme able to tackle both subcritical and supercritical flow and the transitions between them.

The two-dimensional (2Dh) shallow water equations are written as:

$$\frac{\partial \zeta}{\partial t} + \frac{\partial(uh)}{\partial x} + \frac{\partial(vh)}{\partial y} = 0 \quad (3.1)$$

$$\begin{aligned} \frac{\partial u}{\partial t} + u \frac{\partial u}{\partial x} + v \frac{\partial u}{\partial y} + g \frac{\partial \zeta}{\partial x} + c_f \frac{u|U|}{h} &= 0 \\ \frac{\partial v}{\partial t} + u \frac{\partial v}{\partial x} + v \frac{\partial v}{\partial y} + g \frac{\partial \zeta}{\partial y} + c_f \frac{v|U|}{h} &= 0 \end{aligned} \quad (3.2)$$

with:

- u velocity in x-direction
- v velocity in y-direction
- U $\sqrt{u^2 + v^2}$
- ζ water level above plane of reference

- c_f dimensionless resistance factor
- d depth below plane of reference
- h water depth: $\zeta+d$
- g gravitational acceleration term

These equations are non-linear and they describe water motion for which vertical acceleration are small compared to horizontal accelerations (e.g. tidal flow, river flow, flood flow).

Equations 5.1 do not incorporate the turbulent stress terms accounting for the sub grid transfer of momentum in between grid cells. These terms have been omitted. This is justified because they are relatively unimportant for flood flow computations.

The shear stress on the bed for a depth-averaged turbulent flow (2D) in Delft FLS is assumed to be given by a quadratic friction law:

$$\tau = c_f \rho U^2 \quad (3.3)$$

The resistance factor c_f can be described in Delft FLS with the following formulations.

The **Chézy** formulation:

$$c_f = \frac{g}{C^2} \quad (3.4)$$

with C = Chézy coefficient [$m^{1/2}/s$].

The **Manning** formulation:

$$c_f = \frac{g n^2}{h^{1/3}} \quad (3.5)$$

where n is the Manning coefficient [$m^{-1/3}s$].

The **White Colebrook** formulation:

$$\sqrt{\frac{g}{c_f}} = 18 \frac{m^{1/2}}{s} \log \frac{12h}{k_s} \quad (3.6)$$

where k_s is the Nikuradse roughness length [m].

3.3 The numerical approximation of the shallow water equations in Delft FLS

3.1 Introduction

The numerical schemes in Delft FLS are based upon the following characteristics:

- The continuity equation is approximated in such a way that mass is conserved not only globally but also locally and that the total water depth is guaranteed to be always positive. This excludes the necessary of “flooding and “drying” procedures.
- The momentum equation is approximated such that a proper momentum balance is fulfilled also near large gradients.

The combination of positivity of water depths and mass conservation assures a stable numerical solution.

The numerical schemes in Delft FLS distinguish themselves from other numerical schemes that they can tackle flow problems with large gradients, like hydraulic jumps and flooding of initially dry land. Near these discontinuities smooth solutions don't exist and the partial differential equations (PDE) are not valid here. Conservation properties are needed to connect the shallow water equations at both sides of the discontinuity. These properties are satisfied with a proper momentum balance near the discontinuity. As mentioned earlier, the numerical approach of the momentum equation in Delft FLS is strict momentum conservative.

To connect the equations at both sides of the discontinuity, one needs to know the conditions at the sides of the discontinuity. At first section 3.3.2 describes the way in which these conditions are obtained. The next sections describe the numerical methods

3.3.2 Conditions at discontinuities

To obtain the conditions at a discontinuity one considers a region consisting of water lying between two vertical planes $x = a_0(t)$ and $x = a_1(t)$ with $a_1 > a_0$ and such that this planes contains always the same particles, see Figure 3.1. Hence the horizontal velocity component u is the same throughout any vertical plane. One supposes that there is a finite discontinuity in the surface elevation at a point $x = \xi(t)$ inside the region of water between $x = a_0(t)$ and $x = a_1(t)$.

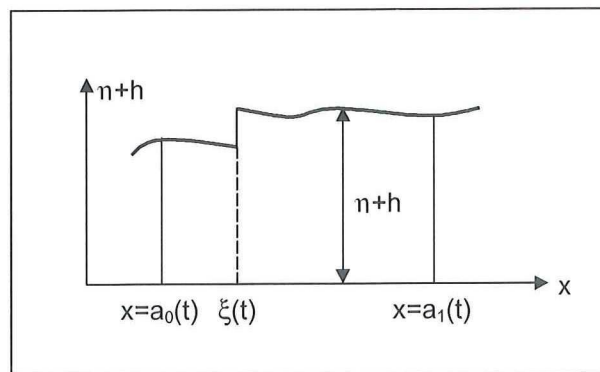


Figure 3.1 Discontinuity in a region of water

If one applies the laws of conservation of mass and momentum to the region of water, the relations yield:

$$\frac{d}{dt} \int_{a_0(t)}^{a_1(t)} \rho(h + \eta) dx = 0 \quad (3.7)$$

and

$$\frac{d}{dt} \int_{a_0(t)}^{a_1(t)} \rho(h + \eta) u dx = \int_{-h}^{\eta_0} p_0 dy - \int_{-h}^{\eta_1} p_1 dy = \frac{1}{2} g\rho(\eta_0 + h)^2 - \frac{1}{2} g\rho(\eta_1 + h)^2 \quad (3.8)$$

The second relation yields that the rate of change of momentum of the water column is equal to the difference of the resulting forces at the end sections of the column. The integrals in these relations have the form:

$$I = \int_{a_0(t)}^{a_1(t)} \psi(x,t) dx \quad (3.9)$$

in which $\psi(x,t)$ has a discontinuity at $x = \xi(t)$. Differentiation and dividing this integral gives:

$$\frac{dI}{dt} = \frac{d}{dt} \int_{a_0(t)}^{\xi(t)} \psi dx + \int_{a_0(t)}^{a_1(t)} \frac{\partial \psi}{\partial t} dx + \psi(\xi_-, t) \dot{\xi}(t) - \psi(a_0(t), t) u_0 + \psi(a_1(t), t) u_1 - \psi(\xi_+, t) \dot{\xi}(t) \quad (3.10)$$

The quantities u_0 and u_1 are the velocities $\dot{a}_0(t)$ and $\dot{a}_1(t)$ at the ends of the column, $\dot{\xi}$ is the velocity of the discontinuity, and $\psi(\xi_-, t)$ and $\psi(\xi_+, t)$ means that the limit values of ψ to the left and the right of $x = \xi$ respectively are to be taken.

Now the limit case is considered in which the length of the column tends to zero such that the discontinuity remains inside the column. This leads for the integral 3.10 to:

$$\lim_{a_1 \rightarrow a_0} \frac{dI}{dt} = \psi_1 v_1 - \psi_0 v_0 \quad (3.11)$$

in which v_1 and v_2 are the relative velocities given by:

$$\begin{aligned} v_1 &= u_1 - \dot{\xi}, \\ v_0 &= u_0 - \dot{\xi} \end{aligned} \quad (3.12)$$

The limit values of ψ to the right and left side of the discontinuity are represented by ψ_1 and ψ_0 respectively. Making use of 3.11 and 3.12 for the limit cases that arise from 3.7 and 3.8 one obtains the following **conditions**:

$$\rho(\eta_1 + h)v_1 - \rho(\eta_0 + h)v_0 = 0 \quad (3.13)$$

and

$$\rho(\eta_1 + h)u_1 v_1 - \rho(\eta_0 + h)u_0 v_0 = \frac{1}{2} \rho g (\eta_0 + h)^2 - \frac{1}{2} \rho g (\eta_1 + h)^2 \quad (3.14)$$

By taking $h_1 = (\eta_1 + h)$ and $h_0 = (\eta_0 + h)$, representing the water depths at both sides of the discontinuity, one obtains the following **shock conditions**:

$$\begin{aligned} \rho h_1 v_1 &= \rho h_0 v_0 = m \\ m(v_1 - v_0) &= \frac{1}{2} \rho g h_0^2 - \frac{1}{2} \rho g h_1^2 \end{aligned} \quad (3.15)$$

with m representing the mass flux across the shock front. To fix the motion on both sides of the shock five quantities are needed; u_1 , u_0 , h_1 , h_0 and the shock velocity $\dot{\xi}$. Applying an energy balance over the region of water and assuming that no energy is gained at the shock this result that one of the velocities u_0 , u_1 or $\dot{\xi}$ can be set to zero to fulfil the equations 3.15.

3.3.3 Numerical approximation of the SWE in Delft FLS (Stelling, 1999)

continuity equation

If one assumes that the bottom is supposed not to be time varying, the continuity equation 3.1 can be rewritten as:

$$\frac{\partial h}{\partial t} + \frac{\partial(hu)}{\partial x} = 0 \quad (3.16)$$

The numerical approximation of the equations is done with the use of the following common staggered grid, here presented only for the x-direction:

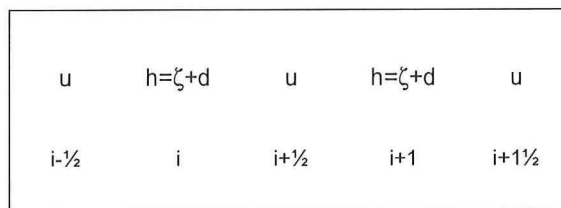


Figure 3.2 Staggered spatial grid

A simple semi-discretisation of 3.16 is given by:

$$\frac{dh}{dt} + \frac{u_{i+1/2} - u_{i-1/2}}{\Delta x} h = 0 \quad \text{at}(i) \quad (3.17)$$

The time discretization of the continuity equation is based on the well-known θ -method. The continuity equation then becomes:

$$\frac{h_i^{n+1} - h_i^n}{\Delta t} + \frac{u_{i+1/2}^{n+\theta} (h_i^n + \Delta h_i) - u_{i-1/2}^{n+\theta} (h_{i-1}^n + \Delta h_{i-1})}{\Delta x} = 0 \quad \text{at}(i) \quad (3.18)$$

$$\text{with } n^{n+\theta} = \theta n^{n+1} + (1-\theta)u^n$$

Δh_i is determined with a *Van Leer slope limiter* as follows:

$$\Delta h_i = \max(0, (\Delta h_1 * \Delta h_2) / (\Delta h_1 + \Delta h_2)), \quad u > 0$$

with:

$$\Delta h_1 = h_{i+1} - h_i, \quad \Delta h_2 = h_i - h_{i-1} \quad (3.19)$$

Equation (3.18) can be rewritten, considering positive flow, as:

$$h_i^{n+1} = h_i^n - \frac{\Delta t \cdot u_{i+1/2}^{n+\theta}}{\Delta x} (h_i^n + \Delta h_i) + \frac{\Delta t \cdot u_{i-1/2}^{n+\theta}}{\Delta x} (h_{i-1}^n + \Delta h_{i-1}) \quad (3.20)$$

with

$$u_{i+1/2}^{n+\theta} \geq 0, \quad u_{i-1/2}^{n+\theta} \geq 0$$

It can now be seen that strict positive water depths are ensured if:

$$\frac{\Delta t \cdot u_{i+1/2}^{n+\theta}}{\Delta x} < 1 \quad (3.21)$$

For the other flow directions similar conditions can be derived. Simply fulfilling equation (3.21) will prevent wet points from drying, so no special drying and flooding procedures are required for this approach. It is to be noticed that the description of the continuity equation is done with the primitive variables instead of the integrated quantities. This description has the advantages that it ensures strictly positive water depths and the upwinding yields artificial viscosity, without influencing strict local mass conservation.

Momentum equation

The numerical advection approximations in the momentum equation are of importance for the conservation properties of the numerical method. As mentioned earlier, *conservation properties are the most important aspect to connect discontinuities in the solution*. The following conservation properties can be considered: mass, momentum and energy. The numerical approximation of the continuity equation (3.16) is already mass conservative.

The energy conservative formulation of equation (3.2) is given by:

$$\frac{\partial u}{\partial t} + \frac{\partial}{\partial x} \left(\frac{1}{2} u^2 + g\zeta \right) + c_f \frac{u|U|}{h} = 0 \quad (3.22)$$

And the momentum conservative formulation of (3.2) is given by:

$$\frac{\partial}{\partial t} (uh) + \frac{\partial}{\partial x} (u^2 h) + gh \frac{\partial \zeta}{\partial x} + c_f u|U| = 0 \quad (3.23)$$

The two equations are equivalent for continuous and smooth solutions. At discontinuities, due to hydraulic jumps or bores, the formulations have no unique solution in general. At this discontinuity extra equations are needed, see section 3.3.2. Conservation of mass and momentum provide in general the internal boundary conditions. However, in case of converging flow, energy head conservative formulation can be applied also.

First the semi discretisation of the energy conservative formulation is given by, assuming positive flow:

$$\Delta x \frac{du}{dt} + 1/2 (u_{i+1/2}^2 - u_{i-1/2}^2) + g(\zeta_{i+1} - \zeta_{i-1}) + c_f \frac{u|u|}{h} = 0 \quad \text{at } (i+1/2) \quad (3.24)$$

Allowing Δx to go to zero and neglecting the friction term, this numerical approximation becomes:

$$\frac{1}{2} u_{i+1/2}^2 - \frac{1}{2} u_{i-1/2}^2 + g\zeta_{i+1} - g\zeta_{i-1} = 0 \quad (3.25)$$

This approximation is first order consistent with the formulation in (3.22), thus energy conservative. This numerical approximation can be applied well for converging flows.

For the numerical approach of the momentum conservation formulation, equation (3.2) is rewritten as, neglecting the friction term:

$$\frac{\partial u}{\partial t} + \frac{1}{h} \left\{ \frac{\partial uuh}{\partial x} - u \frac{\partial uh}{\partial x} \right\} + g \frac{\partial \zeta}{\partial x} = 0 \quad (3.26)$$

This is numerical approximated by assuming a positive flow:

$$\frac{du_{i+1/2}}{dt} + \frac{1}{\bar{h}_{i+1/2}} \left\{ (u_{i+1/2} + \Delta u_{i+1/2}) \bar{q}_{i+1} - (u_{i-1/2} + \Delta u_{i-1/2}) \bar{q}_i - u_{i+1/2} (\bar{q}_{i+1} - \bar{q}_i) \right\} + g \frac{\zeta_{i+1} - \zeta_i}{\Delta x} = 0 \quad (3.27)$$

$$\text{with: } \bar{h}_{i+1/2} = \frac{h_i + h_{i+1}}{2}, \quad \bar{q}_{i+1} = \frac{q_{i+1/2} + q_{i+1/2}}{2}, \quad \bar{q}_i = \frac{q_{i-1/2} + q_{i+1/2}}{2}$$

$\Delta u_{i \pm 1/2}$ is again determined with a *Van Leer slope limiter* as follows:

$$\Delta u_{i+1/2} = \max(0, (\Delta u_1 * \Delta u_2) / (\Delta u_1 + \Delta u_2)), \quad u > 0$$

with:

$$\Delta u_1 = u_{i+1/2} - u_{i+1/2}, \quad \Delta u_2 = u_{i+1/2} - u_{i-1/2} \quad (3.28)$$

The use of this slope limiter provides a second order approximation. The momentum equation (3.16) is now approximated by:

$$\frac{d\bar{h}_{i+1/2}}{dt} + \frac{\bar{q}_{i+1} - \bar{q}_i}{\Delta x} = 0 \quad (3.29)$$

Multiplying equation (3.24) with $\bar{h}_{i+1/2}$ and equation (3.26) with $u_{i+1/2}$ and adding up the results gives, again, assuming positives flows:

$$\Delta x \frac{d(u_{i+1/2} \bar{h}_{i+1/2})}{dt} + \left\{ (u_{i+1/2} + \Delta u_{i+1/2}) \bar{q}_{i+1} - (u_{i-1/2} + \Delta u_{i-1/2}) \bar{q}_i \right\} + g \bar{h}_{i+1/2} (\zeta_{i+1} - \zeta_i) = 0 \quad (3.30)$$

This approximation is second order consistent with the momentum conservative formulation in (3.23). It includes the shock conditions to connect the both sides of the discontinuity.

Consequently, Delft FLS includes the possibility to use various numerical conservation methods. Near discontinuities the momentum conservation method will be used. For converging flows an energy conservation method can be used.

4 Verification of the numerical results

4.1 Introduction

This chapter describes the verification of the computer model Delft FLS using of the data obtained from the physical experiment described in chapter 2.

Section 4.2 and 4.3 describe the verification of the calculated results for both the two wet bed cases and the dry-bed. Section 4.4 contains the conclusions from the verification results.

4.2 Numerical results against experimental results for the wet-bed cases

4.2.1 Input parameters in Delft FLS

The following input parameters were used in the program:

- Grid size, $\Delta x = \Delta y = 0.05$ m;
- time step $\Delta t = 0.005$ s;
- a certain bottom roughness value.

The quadratic friction law used to calculate the bottom shear stress is valid when the flow is turbulent. The Reynolds number indicates if the flow is indeed turbulent. Stoker (1957) gives the following formula to calculate the flow velocity u_1 behind the bore:

$$u_1 = \dot{\xi} \left(1 - \frac{h_0}{h_1} \right) \quad (4.1)$$

with $\dot{\xi}$ the bore speed, h_1 the height of the bore and h_0 the initial water depth upstream with $u_0 = 0$ m/s. With the use of the front bore speeds calculated in section 2.7.2 and the measured water depths from Appendix A this gives a average flow velocity u_1 behind the bore for the 3 cm experiment of about 0.6 m/s. The Reynolds number is now given by:

$$\text{Re} = \frac{uh}{\nu} = \frac{0.6 \text{ m/s} \cdot 0.06 \text{ m}}{10^{-6} \text{ m}^2/\text{s}} \sim 36000 \quad (4.2)$$

The flow is laminar if the Reynolds number is smaller than about 1000. The experimental flow is obviously turbulent, so the use of the quadratic friction law is valid, see formula 3.2.

The Manning formulation is used to calculate the Chézy value. The Manning value n is set to $0.012 \text{ m}^{-1/3}\text{s}$ (Battjes, 1997). This value represents smooth concrete, which was also the case for the bottom material in the physical experiment (see chapter 2, section 2.3.2).

4.2.2 Numerical results for the 3 cm wet-bed case

The following graph shows the numerical results of the model Delft FLS, plotted against the measured positions of the front bore for the wet-bed case with an initial water depth of 3 cm. The measured front bore positions are the same as the front bore positions in Appendix C.

The front bore positions are drawn for the times $t = 1$ s, $t = 2$ s, $t = 3$ s and $t = 4$ s after the start of lifting the gate and only for one half of the basin because of the symmetry of the experiment. The blue dotted line represents the calculated front bore positions and the red line represents the measured front bore positions.

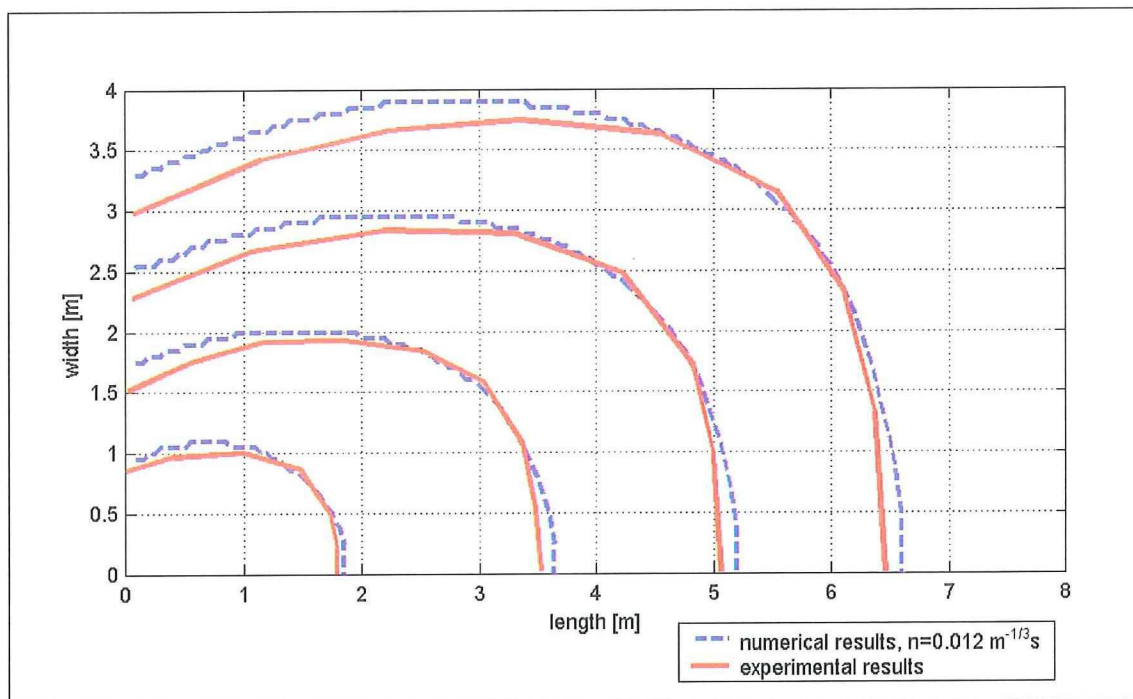
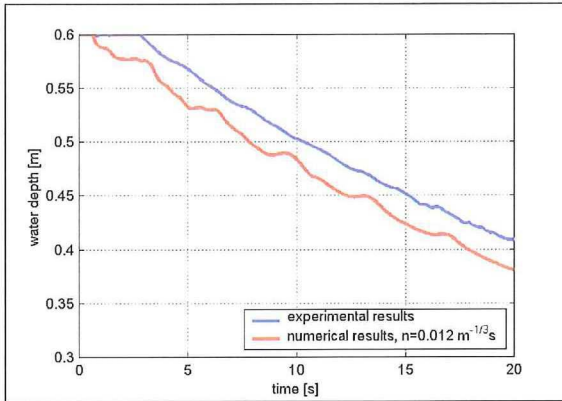


Figure 4.1 Calculated front bore positions and measured front bore positions, initial water depth 3 cm.

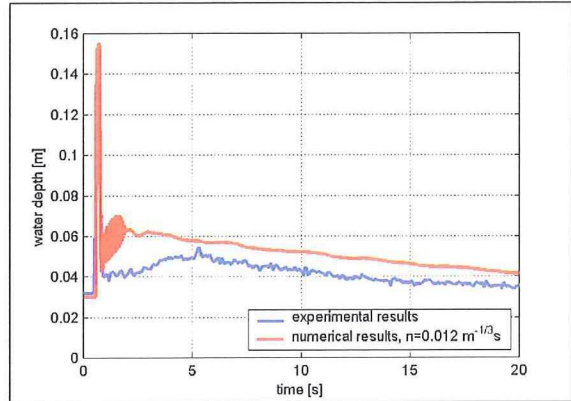
The graph shows a good similarity between the calculations and the measurements for the first 4 seconds of the flow. The experimental flow differs a little bit in the propagation speed in the latitude direction. This is very probably due to the contraction in the aperture, which is underestimated in the numerical model.

The calculated water depths, with $t = 0$ s at the start of lifting the gate, are also a good approximation of the physical reality, see Figure 4.2.

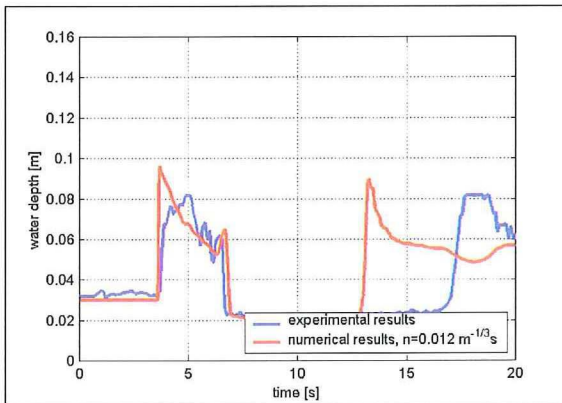
The decrease of the water depth in the reservoir (gauge 00) starts too fast in the simulation. This is probably due to the three-dimensional character of the flow behind the aperture in the physical experiment. Apart from that, the development in time of the calculated water depth and measured water depth in the reservoir are properly the same. This implies that the calculated and measured volume flow Q through the aperture is approximately equal.



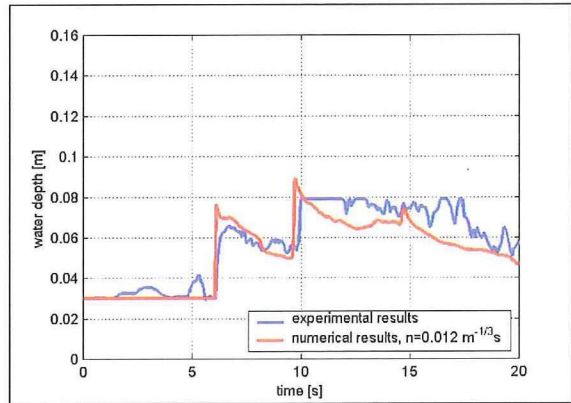
gauge 00 (reservoir)



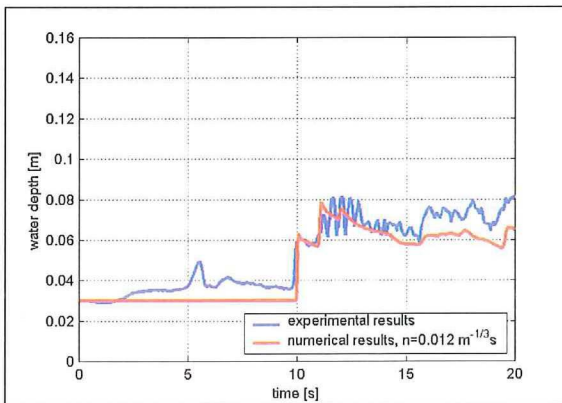
gauge 01 (1 m from the aperture)



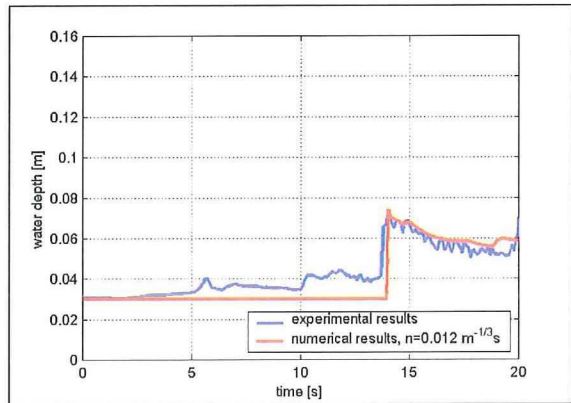
gauge 02 (6 m from the aperture)



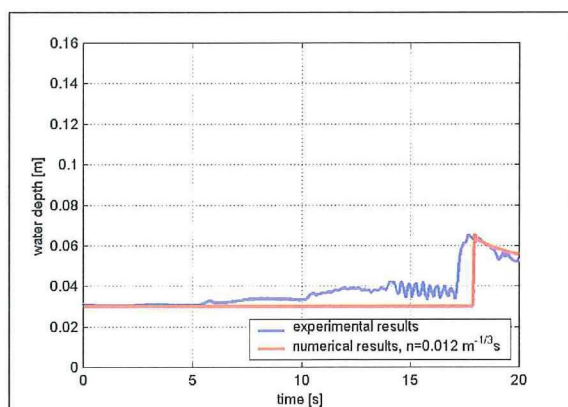
gauge 03 (9 m from the aperture)



gauge 04 (13 m from the aperture)



gauge 05 (17 m from the aperture)



gauge 06 (21 m from the aperture)

Figure 4.2 Calculated water depths and measured water depths, initial water depth 3 cm.

Gauge 02 shows a very good similarity between the calculations and measurements for the location and heights of the hydraulic jump and propagating wave front. The model calculates the water depth of the super critical flow behind the aperture also very accurately. The 'wall' reflected wave reaches gauge 02 too fast in the simulation, but it has anyway the same height as in the measurements.

The propagation speed of the wave front is calculated very well, actually in the far field, after many "chaotic" wall reflected waves.

Friction sensitivity of the experiment

The numerical results of the model discussed above were calculated with a chosen bottom friction value representing smooth concrete. The numerical results approximated the measurements very well. Still a few calculations are made with different bottom friction values to determine the influence of this parameter. The calculations are made with Manning roughness values n of $0.010 \text{ m}^{-1/3}\text{s}$, representing (plexi) glass, $0.020 \text{ m}^{-1/3}\text{s}$, representing boulders (!) and $0.040 \text{ m}^{-1/3}\text{s}$, which what stands for meadows and pastures. The first material, glass, is very smooth and can be seen in relation to the flow conditions as almost frictionless. The calculated front bore positions together with the experimental front bore positions are shown in Appendix E.

It is obvious from the graphs that the bottom roughness value influences the calculated results. If the applied Manning value is too high, like $0.020 \text{ m}^{-1/3}\text{s}$ or $0.040 \text{ m}^{-1/3}\text{s}$, then the calculated front bore positions differ a lot from the experimental front bore positions. The differences between calculations and measurements are logical because these Manning values are, from physical point of view, much too high comparing to the experimental bottom material.

When applying a lower Manning value like $0.010 \text{ m}^{-1/3}\text{s}$, the differences between calculation and measurements are small. This is logical because a Manning value of $0.010 \text{ m}^{-1/3}\text{s}$ corresponds to a Nikuradse roughness length k_s of about 0.0003 m (de Vries, 1999). This value is a much more approximation of the experimental bottom material than a Manning value of $0.020 \text{ m}^{-1/3}\text{s}$, which corresponds to a roughness height of about 0.001 m .

After this, one can conclude that Delft FLS calculates the influence of the bottom friction quite accurate.

4.2.3 Numerical results for the 5 cm wet-bed case

Figure 4.3 shows the results of the 5 cm initial water depth calculations done the model Delft FLS, plotted together with the measured outside front bore positions. The measured front bore positions are the same as the front bore positions in Appendix C.

The graphs show an even better similarity between the calculations and the measurements for the first 4 seconds of the flow than by the experiment with a 5 cm initial water depth. Due to the larger water depth (67 % larger) the bottom friction becomes less important and the flow is more controlled by the advection terms in the momentum equation.

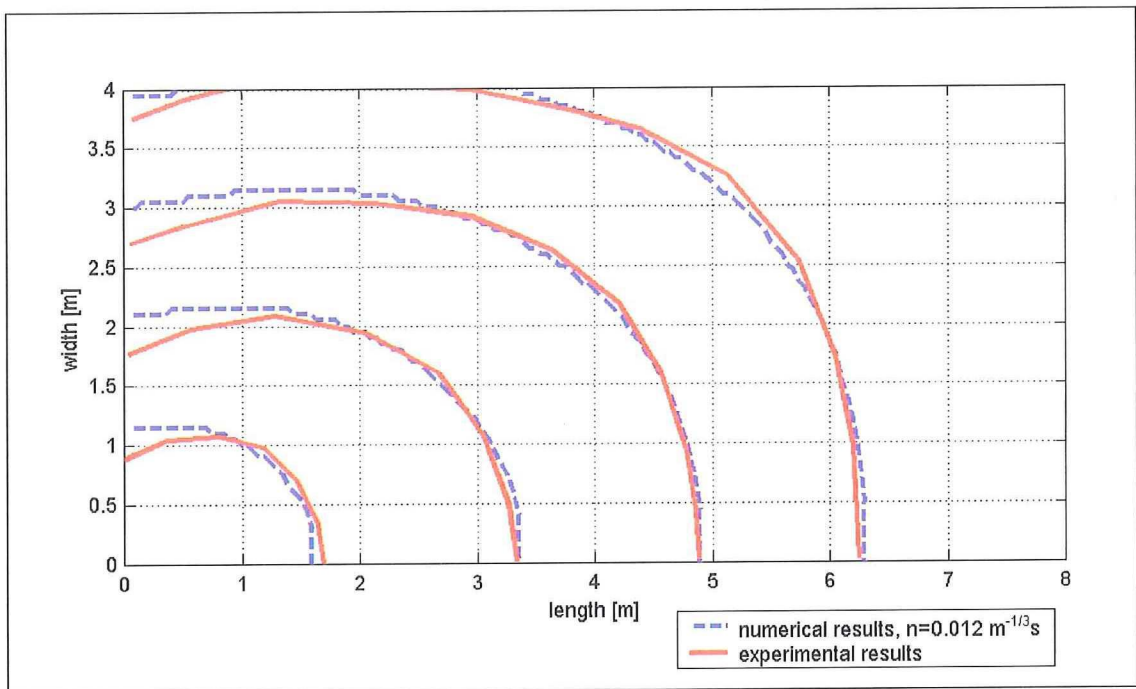
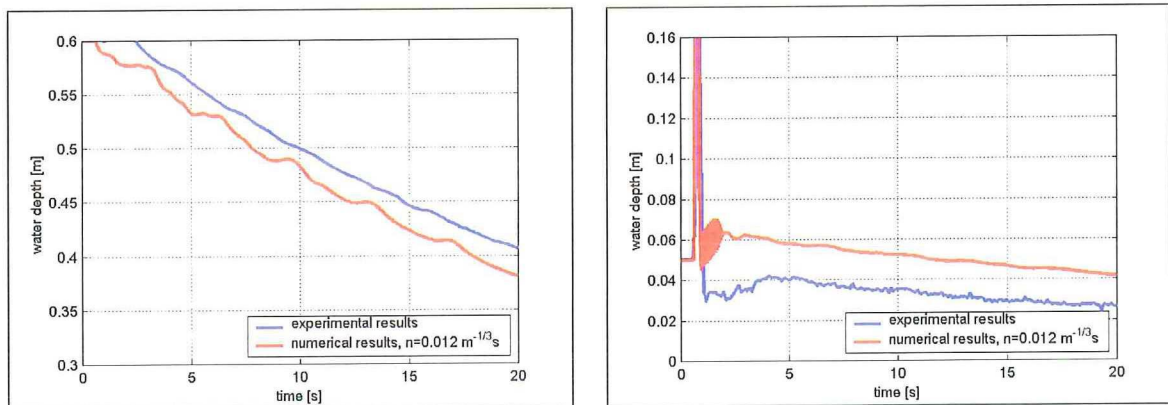


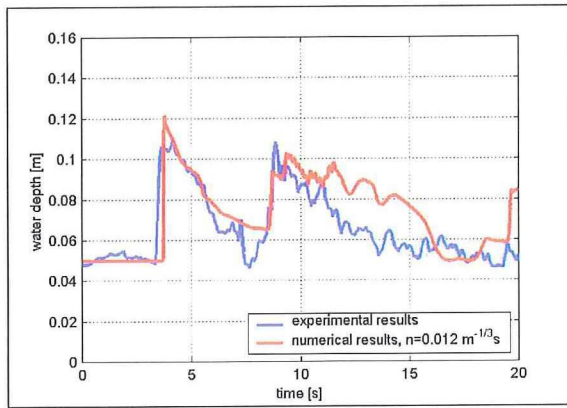
Figure 4.3 Calculated front bore positions and measured front bore positions, initial water depth 5 cm.

Figure 4.4 shows the calculated water depth for an initial water depth of 5 cm:

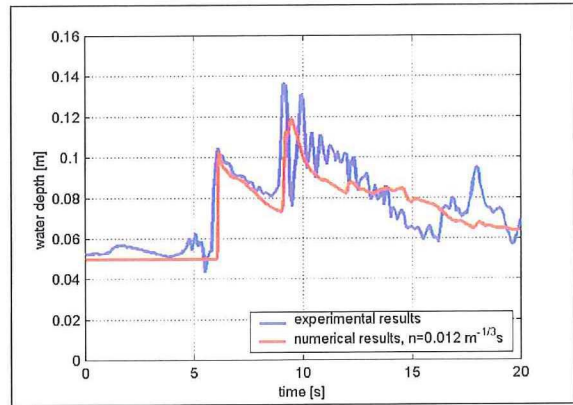


gauge 00 (reservoir)

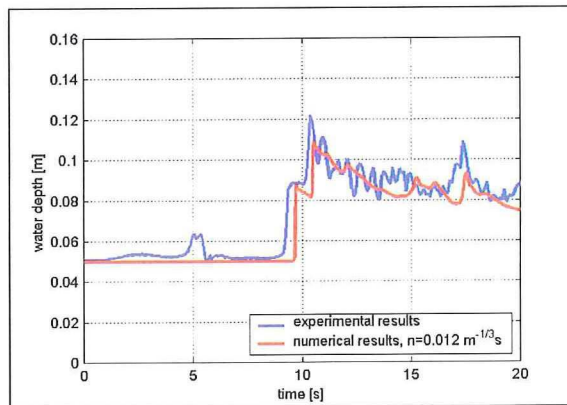
gauge 01 (1 m from the aperture)



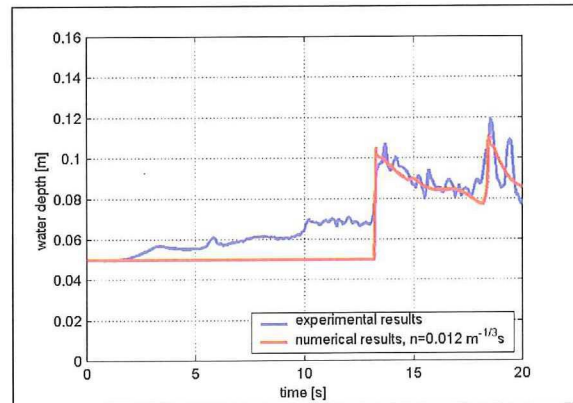
gauge 02 (6 m from the aperture)



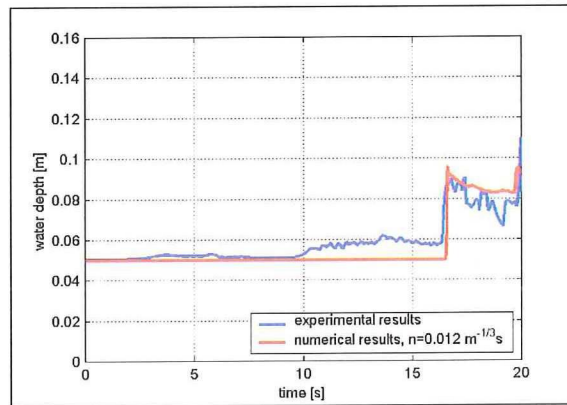
gauge 03 (9 m from the aperture)



gauge 04 (13 m from the aperture)



gauge 05 (17 m from the aperture)



gauge 06 (21 m from the aperture)

Figure 4.4 Calculated water depths and measured water depths, initial water depth 5 cm.

Again, the calculated water depths are a good approximation of the physical reality. The height and propagation speed of the moving wave front, even at a distance from the aperture, are calculated well. The propagation speed of the wall-reflected waves is also calculated correctly.

4.3 Numerical results against experimental data for the dry-bed case

4.3.1 Input parameters in Delft FLS

The following input parameters were used in the program:

- Grid size, $\Delta x = \Delta y = 0.05$ m;
- time step $\Delta t = 0.005$ s;

During the experiment, the average water depth at 1 m from the aperture is about 0.035 m (see gauge 01, Appendix A). The flow velocity at that location is about 2 m/s. The Reynolds number is thus about 70.000 [-] and therefore, the flow at 1 m from the aperture may be supposed to be turbulent, so the use of the quadratic friction law seems valid.

4.3.2 Numerical results for the dry-bed case

The calculations are done with two different Manning roughness values, namely: (smooth concrete) and $n = 0.010$ m^{-1/3}s (glass). The trench cover in the bottom is represented by a Manning roughness value of 0.010 m^{-1/3}s. The Figures 4.5 and 4.6 show the calculated outside front bore positions of the flow and the experimental outside front bore positions respectively for $n = 0.012$ m^{-1/3}s and $n = 0.010$ m^{-1/3}s.

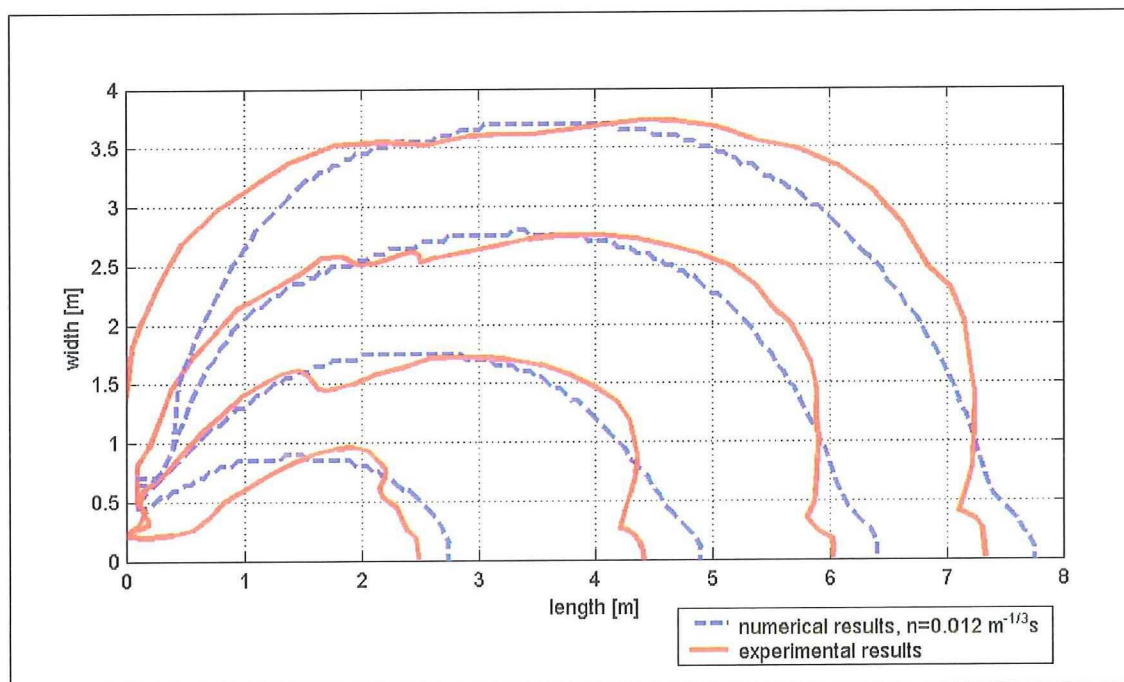


Figure 4.5 Calculated front bore positions and measured front bore positions, $n = 0.012$ m^{-1/3}s

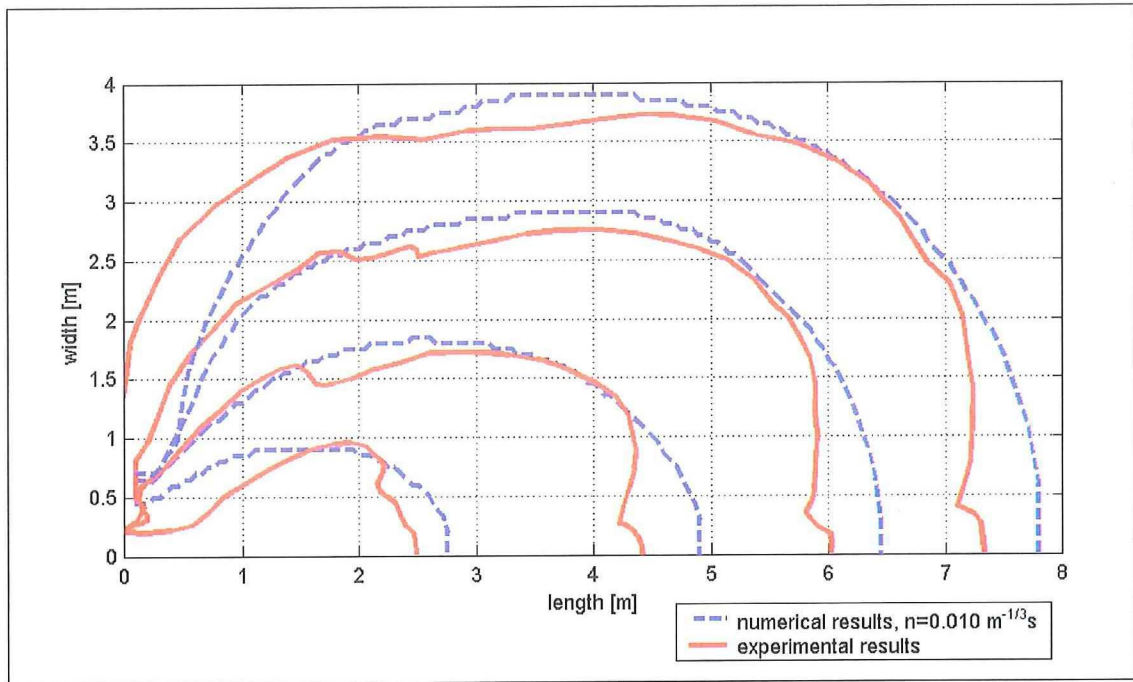
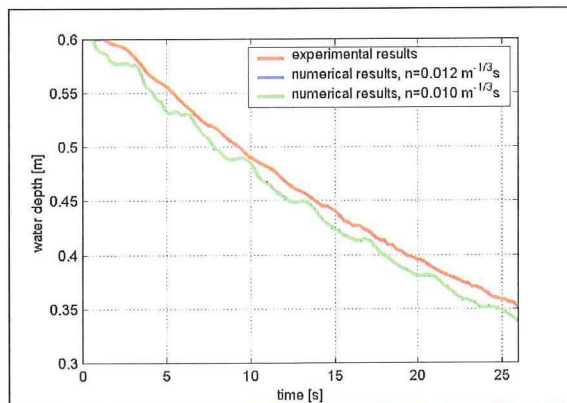


Figure 4.6 Calculated front bore positions and measured front bore positions, $n = 0.010 \text{ m}^{-1/3} \text{ s}$

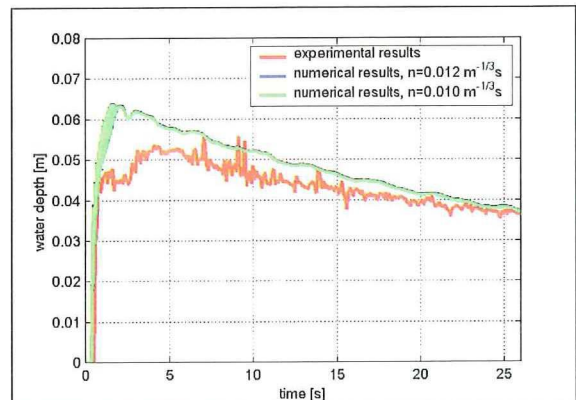
As in the wet-bed case, the graphs show a remarkably good similarity between the calculated and experimental front bore positions for both Manning values. The influence of the discontinuity in the bottom roughness in the experimental front bore positions, as well as in the calculated front bore positions with $n = 0.012 \text{ m}^{-1/3} \text{ s}$. The front bore positions calculated with a Manning roughness value of $0.010 \text{ m}^{-1/3} \text{ s}$ show a better similarity with the experimental results than with the calculated results with a Manning value of $0.012 \text{ m}^{-1/3} \text{ s}$.

This is not entirely consistent with the conclusions made in section 4.2: a Manning value of $0.012 \text{ m}^{-1/3} \text{ s}$, representing smooth concrete, which was also present in the experiment, gave the best simulation results for the wet-bed cases.

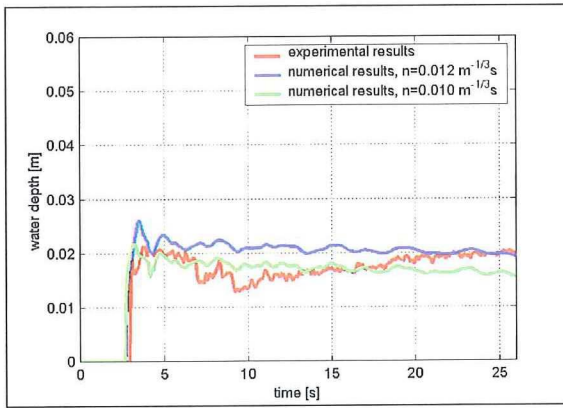
The water depths calculated with a Manning roughness value of $0.010 \text{ m}^{-1/3} \text{ s}$ show also a better similarity with the experimental data than these calculated with a Manning value of $0.012 \text{ m}^{-1/3} \text{ s}$, see Figure 4.7.



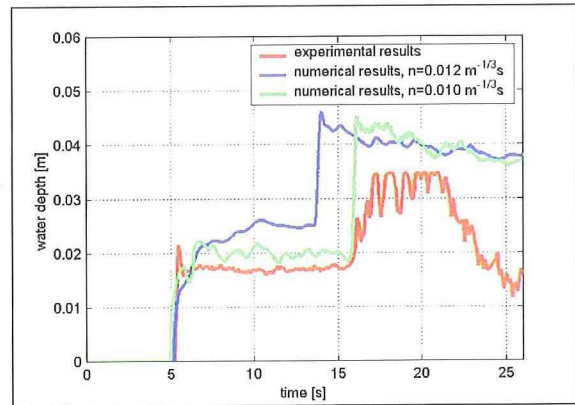
gauge 00 (reservoir)



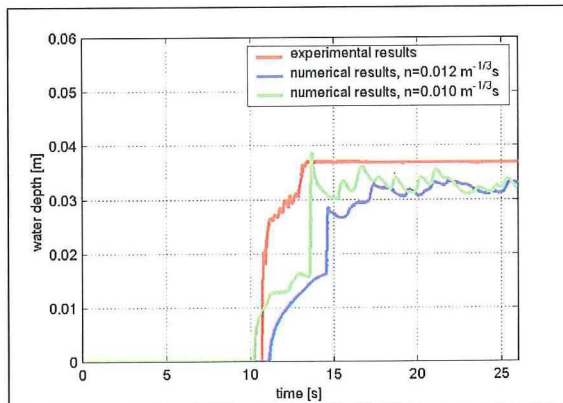
gauge 01 (1 m from the aperture)



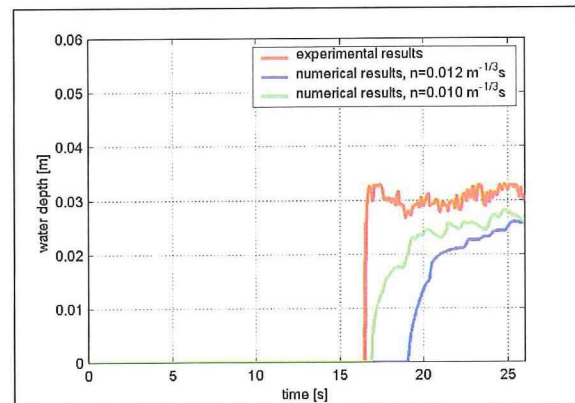
gauge 02 (6 m from the aperture)



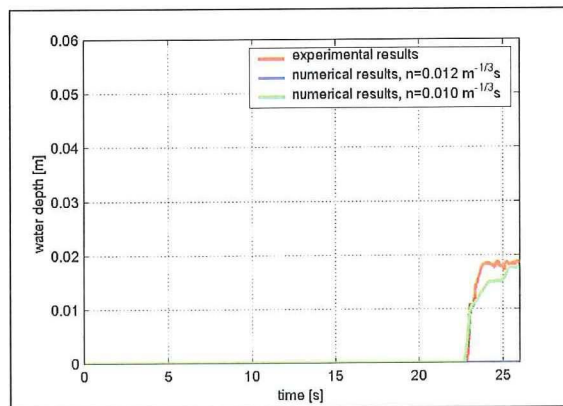
gauge 03 (9 m from the aperture)



gauge 04 (13 m from the aperture)



gauge 05 (17 m from the aperture)



gauge 06 (21 m from the aperture)

Figure 4.7 Calculated water depths and measured water depths (dry-bed case)

Especially at a greater distance from the aperture, the difference between the two calculations increases. Probably, in the case of dry-bed flooding, the used bottom roughness value needs special attention.

Dressler (1975) did some research to the applicability of the Chézy resistance function, always measured in steady flows, to describe highly time-dependent flows such as, for example, dike and dam-break flows over initially dry land, which is also the case in the physical experiment.

The classical dam-break wave solution, based upon the Saint Venant equations, fails to describe accurately the actual physical flow because of the neglect of frictional and turbulent resistive effects. In 1952 Dressler developed a theory that solved the Saint Venant equations including the resistive effects. In this theory, the presence of a special 'tip' region bordering the wave front was pointed out. Whitham (1953) did the same sort of research, and the two formulae for calculating the velocity of the wave front were in almost perfect agreement with each other.

Dressler executed in 1975 three experiments to measure very accurately the trajectories of the forward wave front (the "tip") over time intervals with different bottom roughness values. Smooth wood, coarse sandpaper and wooden slats represented these roughness values. The water slopes, water depths and discharge rates were also measured for each experiment. He calibrated his mathematical model by calculating a resistance factor c_f for each experiment, such that his theoretical results corresponded with the experimental results. This resistance factor c_f deviated in a consistent way from the resistance factor used in the always used for steady flows. This indicated more generally that the Chézy resistance function is probably inadequate to describe highly unsteady flow or the nature of turbulent resistance in the region of a wave front. Dressler found out that a Chézy value of almost 24 percent more than the used value in the Chézy resistance function would be needed to obtain agreement between the measurements and the mathematical results. This tendency is also visible in the simulation results of Delft FLS because the difference between calculated and experimental data is a little smaller when applying a lower roughness value than the one physically present. The calculated results with a Manning value of $0.010 \text{ m}^{-1/3}\text{s}$ show a little better similarity with the experimental results than these calculated with a Manning value of $0.012 \text{ m}^{-1/3}\text{s}$.

4.4 Conclusions drawn from the verification

After comparing the numerical results with the experimental results for the different wet-bed cases, the following conclusions can be drawn:

- The computer model Delft FLS calculates the flow into a filled basin after lifting a vertical gate with considerable accuracy;
- the developments in time of the front bore positions are calculated well for different initial water depths in the basin;
- the calculation of the height and speed of the propagating bore, maintains accurate after several wave reflections;
- the model calculates with a high precision the location and height of a hydraulic jump even in a situation with flow in different directions. This implies that the applied numerical approximation of the momentum equation is conservative;
- the contraction in the aperture is underestimated. This is probably due to a 3D-effect

The following conclusions can be drawn after comparing the simulation results with the experimental results for the dry-bed case:

- In general, Delft FLS simulates accurately the flooding of a dry basin after lifting a vertical gate. This applies to the front bore positions and to the water depths;
- the model is accurate in simulating the height and propagation speed of reflected waves;

- when simulating flow over initially dry land, one must pay special attention to the bottom roughness value used in the model;

5 Conclusions and recommendations

5.1 Conclusions

5.1.1 General

In general it can be said that Delft FLS is able to simulate a highly dynamic two-dimensional flow over a horizontal surface with high accuracy, for an initially dry surface as well as an initially wet surface.

- Discontinuities in a flow like the speed and height of the propagating bore and the height and location of the hydraulic jump are a severe test for numerical models. The numerical approximation must at one moment be energy conservative and at another moment momentum conservative. *Delft FLS* handles both methods correctly, which results in accurate computations for two-dimensional flow.
- Flooding of initially dry land can also be seen as a discontinuity in the flow. The numerical approximation of the continuity and momentum equations ensures always a positive total water depth and calculates also the propagation speed accurately in all directions. This applies to the dynamic part of the flow, as well as the far field, quasi-stationary part of the flow.

5.1.2 Practical

Delft FLS can be used as a reliable simulation tool in case of a dam-break between a buffer basin ('spaarbekken') and the adjoining lake or river. It gives a good simulation of the speed and height of the propagating wave front into the lake or river

The program *Delft FLS* can not only be used to simulate flooding. The program is also very useful to simulate water-regulating systems, like:

- sluices with vertically moving floodgates;
- intake systems in canals and rivers.

5.2 Recommendations

- The executed experiment is done on a small scale. It contained a dynamic and quasi-static flow, which was a severe test of the model. The reflected waves from the boundary of the basin were also calculated correctly. However, a real scale test with many obstacles in the flow would give also useful information to verify the model.
- The experiments were executed with one bottom roughness (smooth concrete). The numerical results were satisfying for both the wet-bed and the dry-bed cases. However, in case of the dry-bed calculations, the use of a representative bottom roughness value needs special attention. Small-

scale physical experiments with different bottom roughness will give useful information about the validity of the used friction formulas in the model to calculate the flow velocity at the tip of the wave.

- The dike-break was simulated in the physical experiment by lifting a vertical gate with a speed of 16 centimetre per second. This method gave a flow downstream of the aperture with a dominating velocity in the direction perpendicular to the aperture. In most of the events this represents not a physical dike-break. In case of a physical dike-break one can assume that the downstream flow is more axial symmetric. Executing an experiment with a decreasing dam or dike height gives a more realistic flow after a dike-break, although one must realise that this is certainly not a more severe test for the program.

References

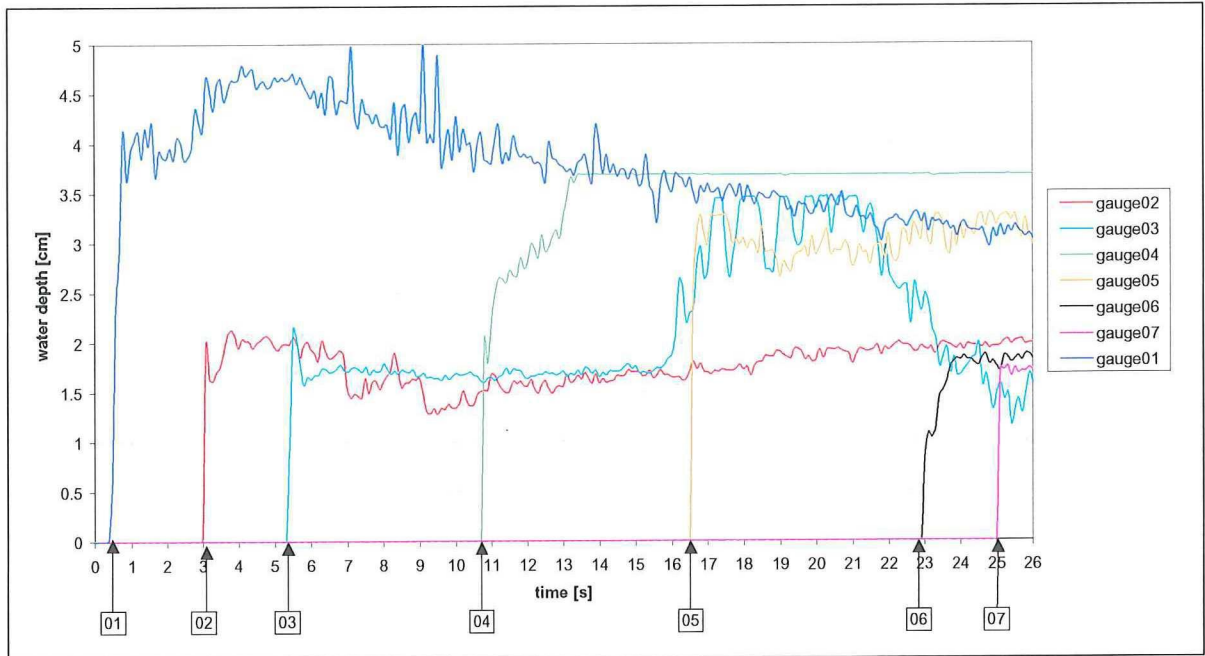
- Akker, C., 1995. Hydrologie. Lecture notes, Delft University of Technology, Delft, The Netherlands.
- Battjes, J.A., 1997. Vloeistofmechanica. Lecture notes, Delft University of Technology, Delft, The Netherlands.
- Battjes, J.A., 1998. Stroming in waterlopen. Lecture notes, Delft University of Technology, Delft, The Netherlands.
- Booij, R., 1992. Turbulentie in de waterloopkunde. Lecture notes, Delft University of Technology, Delft, The Netherlands.
- Chaudry, M.H., 1993. Open-channel flow. Prentice Hall, New Jersey, USA.
- De Vries, M.J., 1999. Flooding. Master thesis, Delft University of Technology, Delft, The Netherlands.
- Dressler, R.F., 1975. Comparison of theories and experiments for the hydraulic dam-break wave, National Bureau of Standards, Washington, D.C., USA.
- Fennema, R.J., 1985. Numerical solution of two-dimensional transient free-surface flows, PhD dissertation, Washington State University, Washington, USA.
- Fontijn, H.L., and Kranenburg C., 1985 Wave propagation after a dike-break. Deelstudie naar een pompaccumulatie, Delft University of Technology, Delft, The Netherlands.
- Kernkamp, H.W.J., 2001. Manual Delft FLS 2.55. WL | Delft Hydraulics, Delft, The Netherlands.
- Soares Frazão, S., 1998. Description of Test case 1: channel with 45° bend. Université catholique de Louvain, Louvain, Belgium
- Soares Frazão, S. et al., 1998. Dam-break flow through sharp bends, Physical model and 2D Boltzmann model validation. Université catholique de Louvain, Louvain, Belgium
- Stelling, G.S., 1999. A Numerical Method for Inundation Simulation. WL | Delft Hydraulics / Delft University of Technology, Delft, The Netherlands.
- Stoker, J.J., 1957. Water waves. Pure and applied mathematics vol. IV, Interscience Publishers, New York, USA.
- Visser, P.J., 1998. Breach growth in sand-dikes. PhD dissertation, Delft University of Technology, Delft, The Netherlands.
- Zoppou, C and Roberts, S. Numerical solution of the two-dimensional unsteady dam-break. Applied Mathematical Modelling vol. 24 (2000).

Appendices

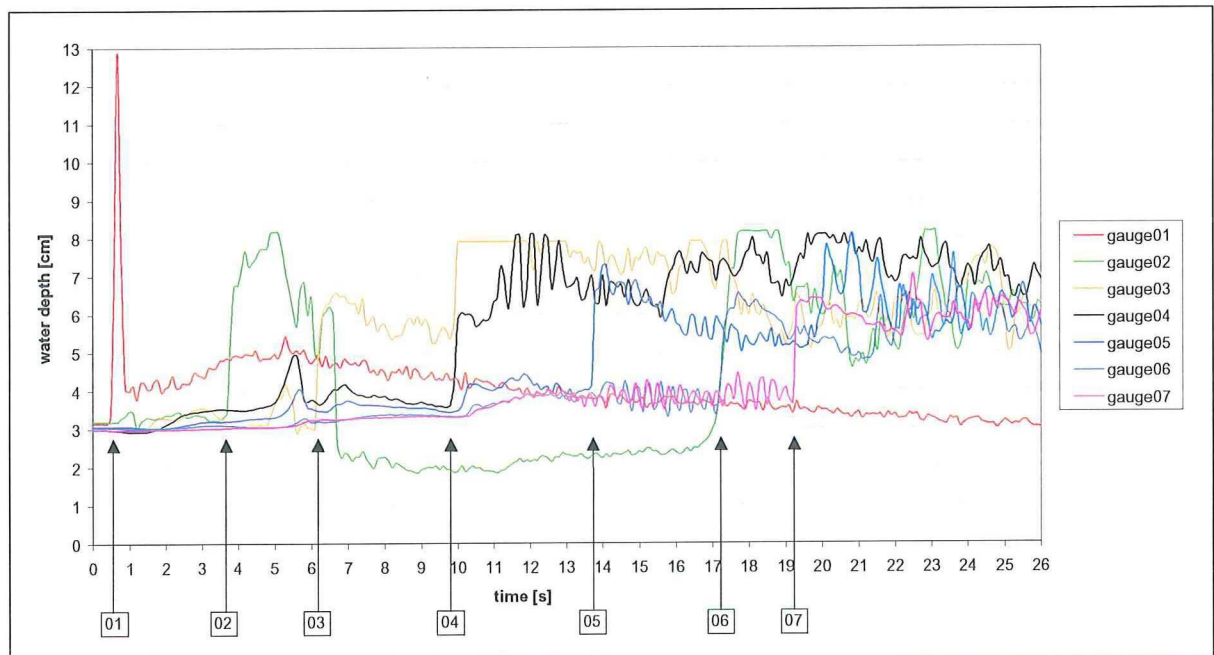
- A Measured water depths**
- B Measured front bore positions**
- C Front bore positions in the horizontal plane**
- D Roughness values of a number of bottom materials**
- E Bottom friction sensitivity in the experiment**

A Measured water depths

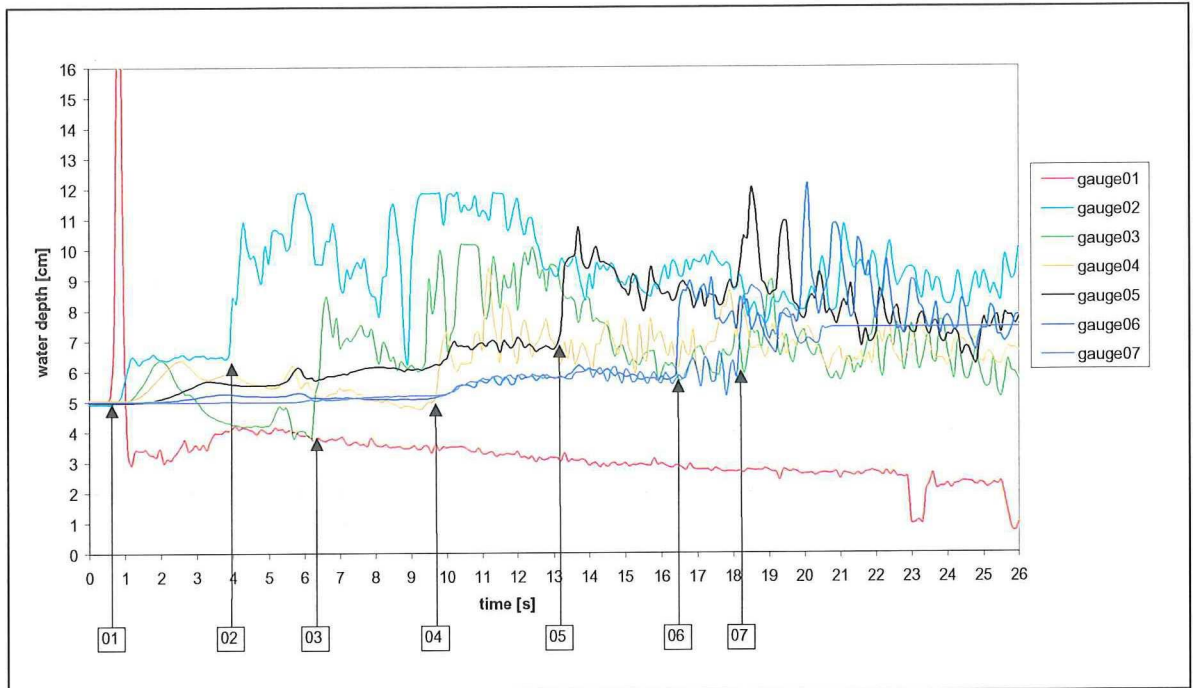
DRY-BED EXPERIMENT



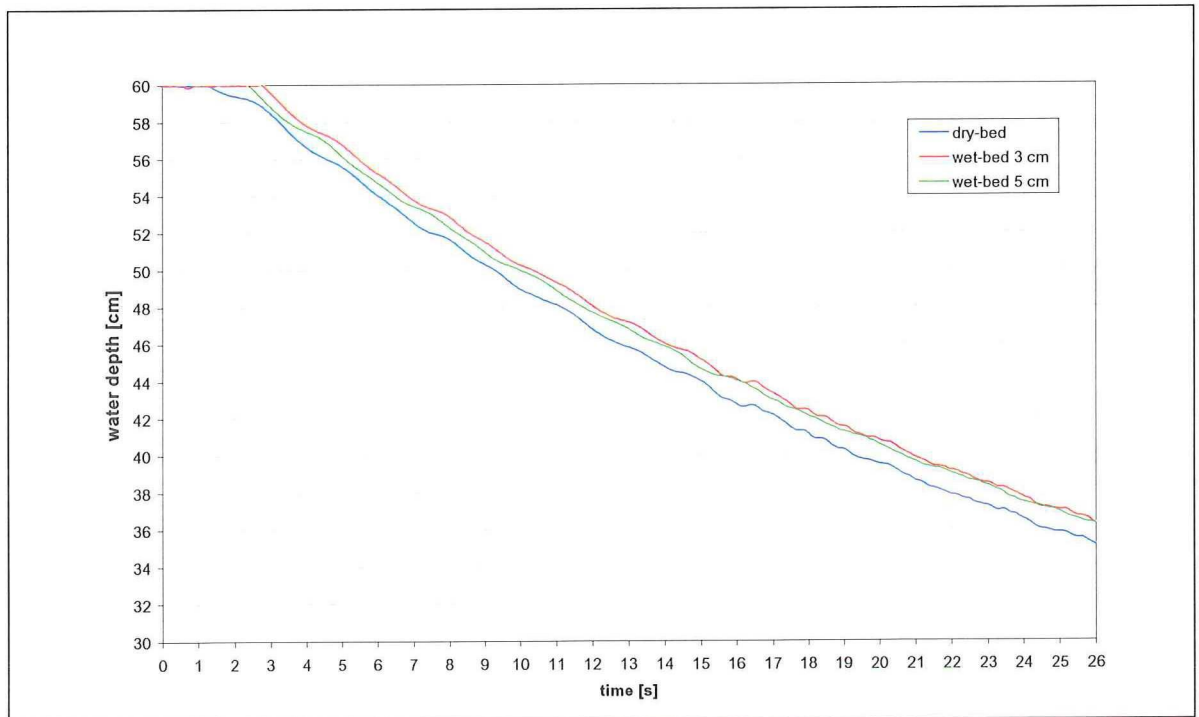
WET-BED EXPERIMENT WITH AN INITIAL WATER DEPTH OF 3 CM



WET-BED EXPERIMENT WITH AN INITIAL WATER DEPTH OF 5 CM



WATER DEPTHS IN THE RESERVOIR

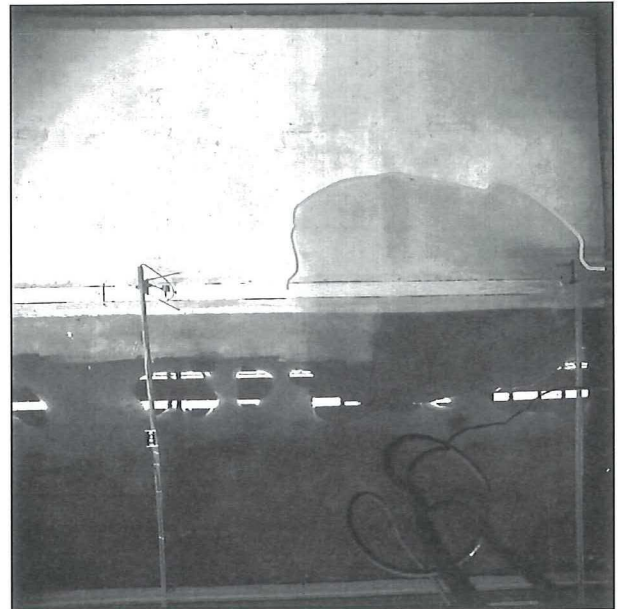


B Measured front bore positions

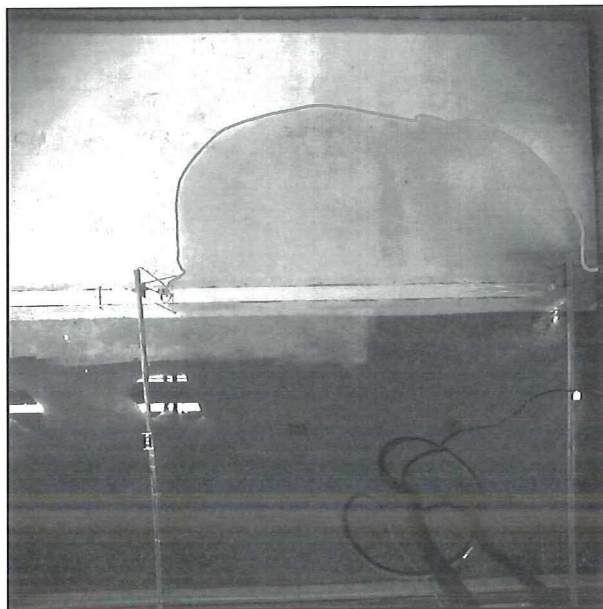
DRY-BED EXPERIMENT



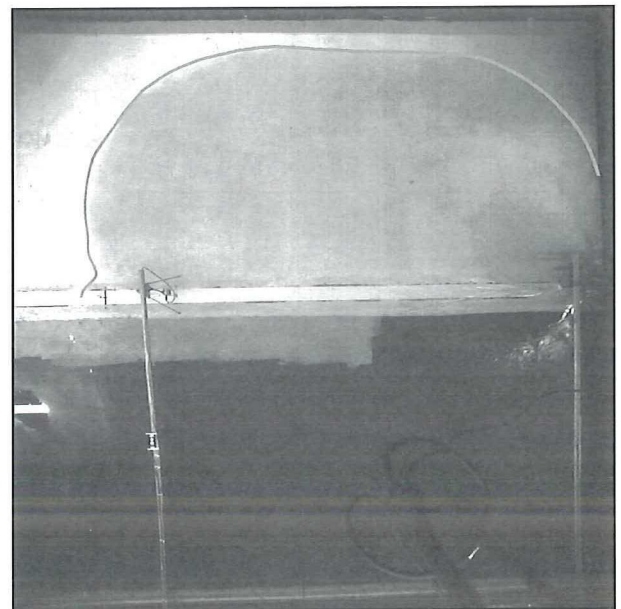
front bore position at $t = 1$ s



front bore position at $t = 2$ s

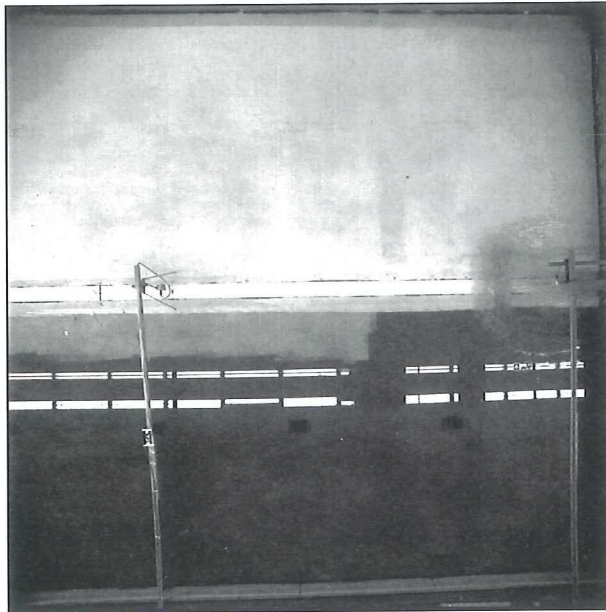


front bore position at $t = 3$ s

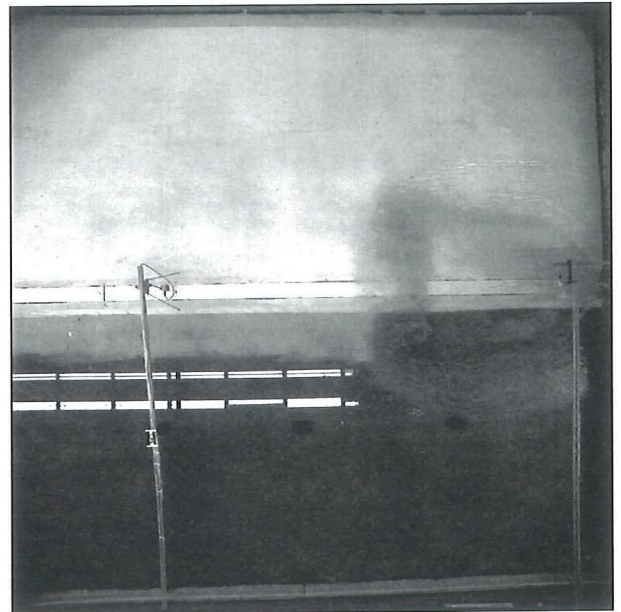


front bore position at $t = 4$ s

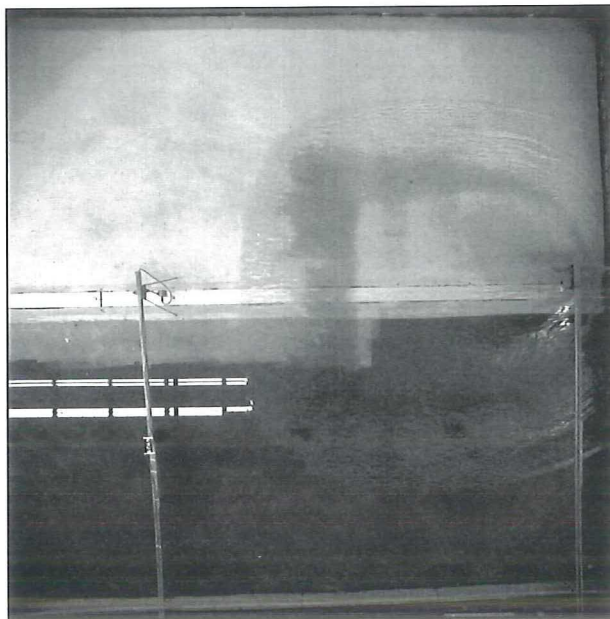
WET-BED EXPERIMENT WITH AN INITIAL WATER DEPTH OF 3 CM



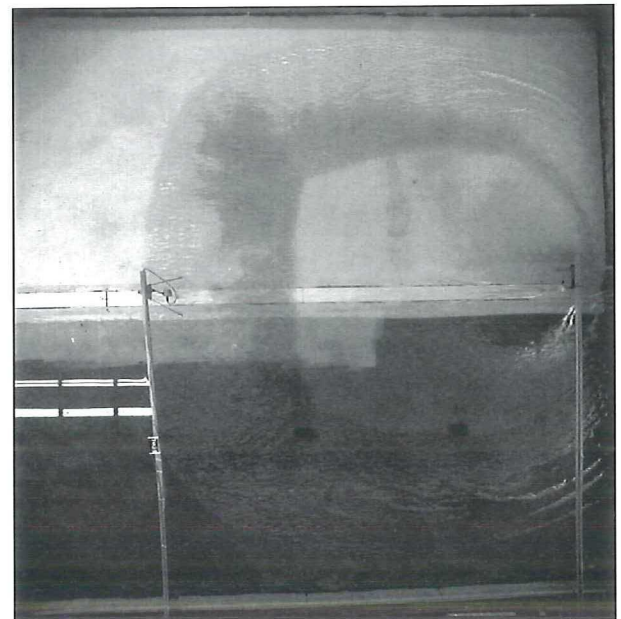
front bore position at $t = 1$ s



front bore position at $t = 2$ s

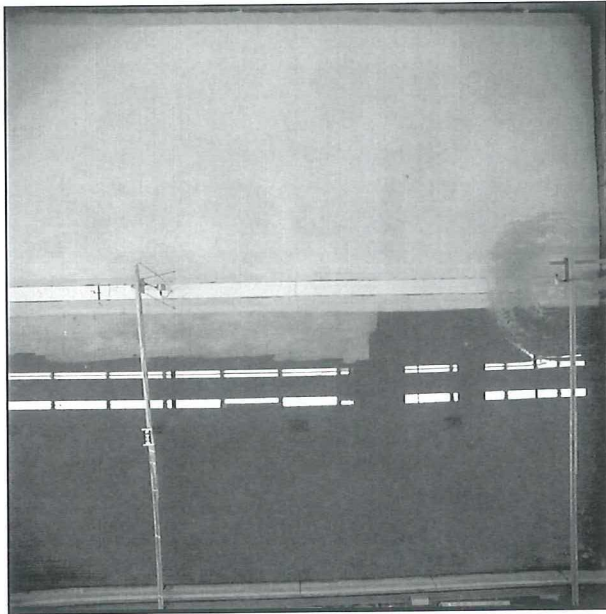


Front bore position at $t = 3$ s

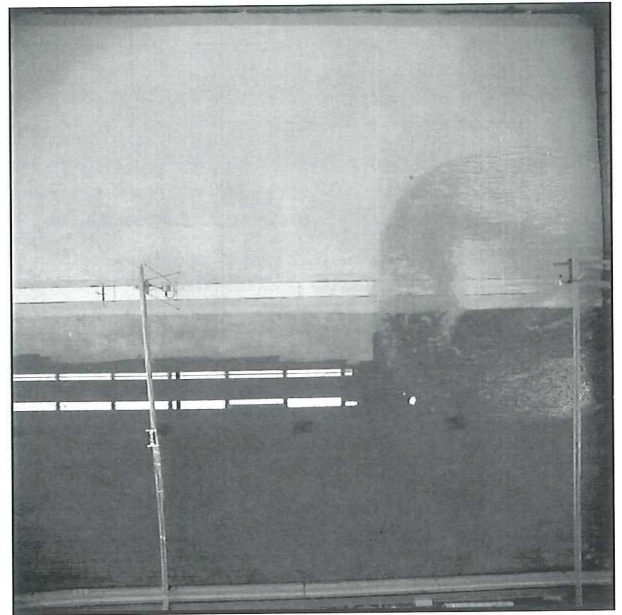


Front bore position at $t = 4$ s

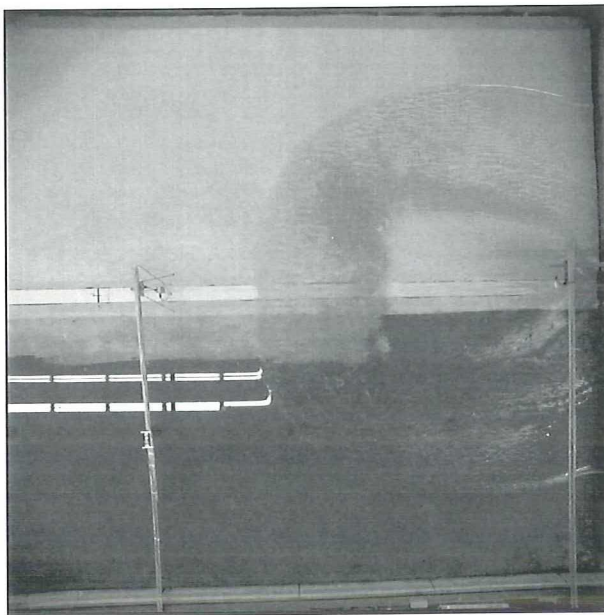
WET-BED EXPERIMENT INITIAL WATER DEPTH 5 CM



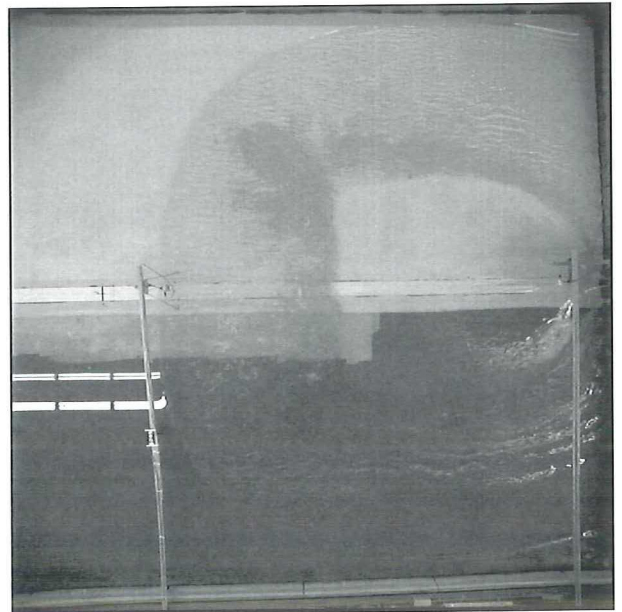
front bore position at $t = 1$ s



front bore position at $t = 2$ s

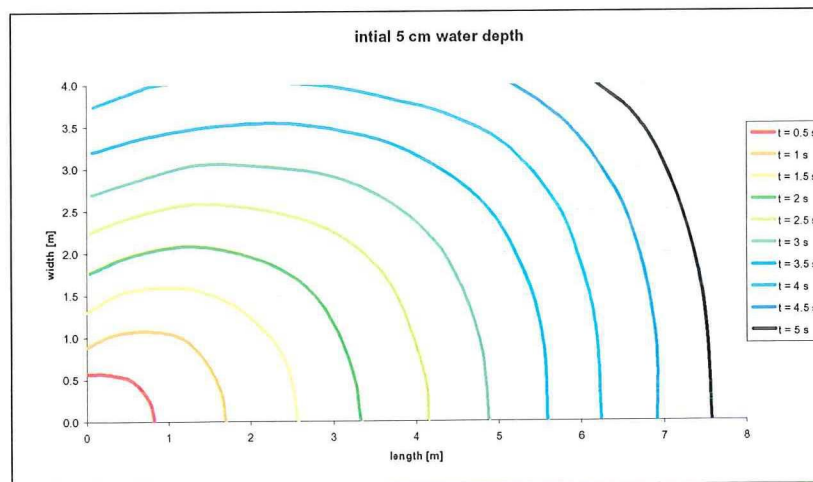
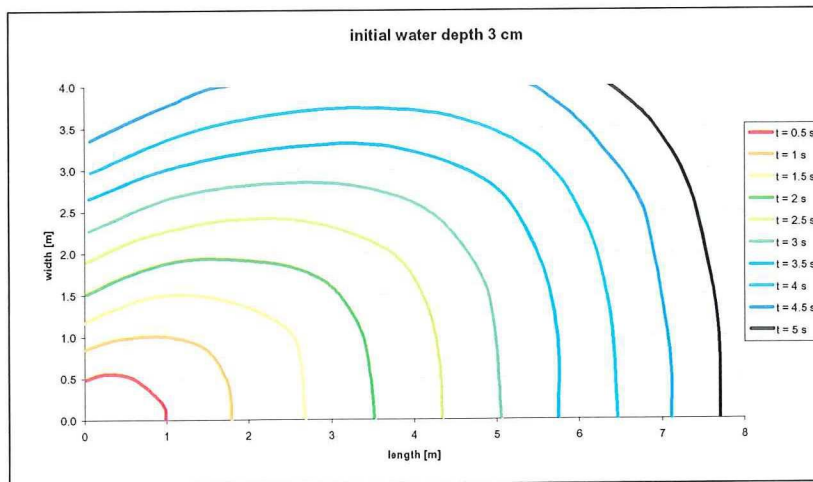
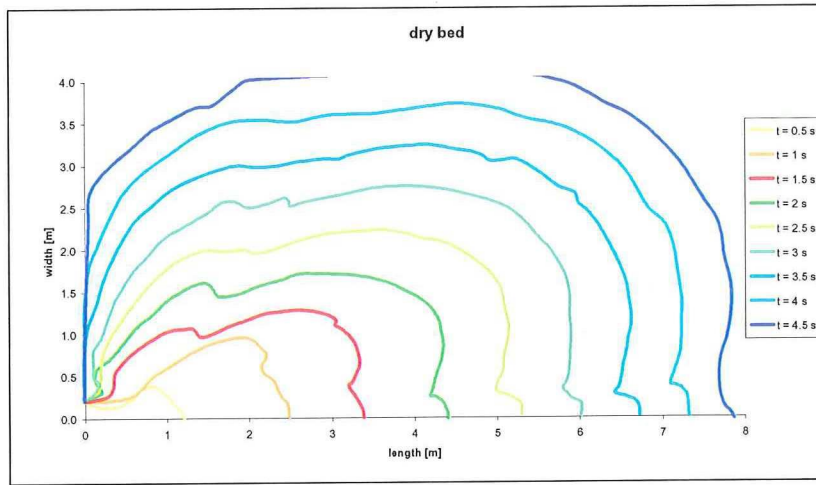


Front bore position at $t = 3$ s



Front bore position at $t = 4$ s

C Front bore positions in the horizontal plane



D Roughness values of a number of bottom materials

Compiled from Battjes (1997), Akker (1995) and Chaudry (1993)

Material	Manning value n [$m^{-1/3}s$]	Nikuradse roughness length k_s [m]
PVC, Plexiglas	0.01	0.00003
Glass	0.01	0.00003
concrete (from rough to smoothed)	0.014 - 0.01	0.02 – 0.0007
Masonry	0.025	0.07 – 0.006
Gravel	0.020 – 0.030	
cobbles with large boulders	0.050	
natural waterways:		0.04 – 0.15
straight, well maintained	0.025 – 0.030	
winding, well maintained	0.035 – 0.040	
winding, with vegetation	0.040 – 0.050	
stones and vegetation	0.050 – 0.060	
meadows, pastures	0.035	0.03 – 0.04
Agriculture	0.040	
shrubs, bushes	0.050	0.4
dense shrubs	0.070	
dense forest	0.100	

E Bottom friction sensitivity in the experiment

